運輸省港湾技術研究所

港湾技術研究所報告

REPORT OF THE PORT AND HARBOUR RESEARCH INSTITUTE

MINISTRY OF TRANSPORT

VOL. 10 NO. 1 MAR. 1971

NAGASE, YOKOSUKA, JAPAN

港湾技術研究所報告は第7巻第1号より年4回定期的に刊行する。
報告の入手を希望する方は論文番号を明記して港湾技術研究所長に申し込んで下さい。

The Report of the Port and Harbour Research Institute is published quarterly, either in Japanese or in occidental languages. The title and synopsis are given both in Japanese and in occidental languages.

The copies of the Report are distributed to the agencies interested on the basis of mutual exchange of technical publication.

Inquiries relating to the Report should be addressed to the director of the Institute specifying the numbers of papers in concern.

港湾技術研究所報告 (REPORT OF P.H.R.I.)

第10巻 第1号 (Vol. 10, No. 1), 1971年3月 (Mar. 1971)

目　　次 (CONTENTS)

1. An Experimental Study of the Turbulent Structure of Wind over Water Waves ……Hajime KATO, Kikuo SANO…… 3

(水面波上の風の乱流構造に関する実験的研究……加藤　始・佐野喜久雄)

2. 波浪データの集中処理方式について
……高橋智晴・鈴木禧実・佐々木　弘
副島　毅・菅原一晃・中井徹也…… 43

(On a Concentrative Handling and Analysis System for Wave Observation Data
……Tomoharu TAKAHASHI, Yoshimi SUZUKI, Hiroshi SASAKI and Takeshi SOEJIMA, Kazuteru SUGAHARA, Tetsuya NAKAI)

3. 粘土試料のかく乱に関する研究（第3報）
—単純せん断試験機による繰り返し破壊試験および圧密試験—
……奥村樹郎・梅田裕史・成田　実…… 77

Studies on the Disturbance of Clay Samples (3rd Reports)
—Repeated Loading Tests and Consolidation Tests with a Simple Shear Apparatus—
……Tatsuro OKUMURA, and Hirofumi UMEAD, Minoru NARITA)

4. 数値解による杭の横抵抗の基準曲線の作成
……山下生比古・稲富隆昌・小蔵紘一郎・奥山育英……107

(New Standard Curves in the PHRI Method ……Ikuhiko YAMASHITA, Takamasa INATOMI, Koichiro OGURA and Yasuhide OKUYAMA)

5. 掘削時における砂の応力—ひずみ関係の一考察
……岩崎峯夫・麻山和正・石塚浩次・河野　茂……169

(Study on the Stress-strain relationship of soils under excavation
……Mineo IWASAKI, Kazumasa ASAYAMA, Kozi ISHIZUKA and Sigeru KONO)

REPORT OF THE PORT AND
HARBOUR RESEARCH INSTITUTE
Vol. 10 No. 1 (Mar. 1971)

1. An Experimental Study of the Turbulent Structure of Wind over Water Waves

Hajime KATO*
Kikuo SANO**

Synopsis

By the use of an X-array hot-wire system and the digital method, the measurements have been made of the horizontal and vertical wind velocity fluctuations, u' and w', over the three kind of waves in a wind-wave tunnel. The cross spectral analyses with respect to u' and w' were extensively used mainly to detect the wave-induced Reynolds stresses. In the first cases, where only mechanically generated long waves existed by the application of soap into water, the phase averaging were effectively used to obtain the wave-induced velocity components. When the wave height H was small (H=1.1 cm), only the positive wave-induced Reynolds stresses were found at the small height above the wave crests. For the wave heights as large as H=6.0 or 7.0 cm, however, the negative wave-induced stresses were prevailing over most of the height except the very small height above the crests where the stresses were positive. In the second cases of wind-waves only, the wave-induced velocity fluctuations also existed considerably at the lowermost measurement height. However they were almost 90° out of phase and did not make much contribution to the $u'w'$-cospectra, that is, to the total Reynolds stresses. Nevertheless the cospectra obtained in winter showed signs of the negative stress. Although the seasonal differences, not only quantitative but qualitative, in the values of $-\overline{u'w'}$ were found, the results obtained at the seasons other than summer indicated that the turbulent Reynolds stresses are nearly constant over the short distances close above the wave crests. It was further found that the turbulent Reynolds stresses at those heights are in reasonably good agreement with the surface shear stresses estimated by applying the log-law to the lowest portion of the wind velocity profiles. In the third cases, where the larger mechanically generated waves and smaller wind waves coexisted, only the negative wave-induced Reynolds stresses of non-negligible magnitude were found regardless of the season, and the turbulent velocity fluctuations were predominant even at the lowermost measurement height somewhat in contrast to the first cases.

* Chief, Storm Surge and Tsunami Laboratory, Hydraulics Division.
** Member of Hydraulic Laboratory, Hydraulics Division.

港湾技術研究所報告
第10巻 第1号 (1971. 3)

1. 水面波上の風の乱流構造に関する実験的研究

加藤 始*・佐野喜久雄**

要 旨

2台の熱線風速計とX-型エレメントを使い，デイジタルのデータ記録処理方式により，風洞水路において3種類の波の上での風速の水平，垂直変動成分 u', w' の測定を行なった。主として，波により誘起されたレイノルズ応力 (wave-induced Reynolds stress) の存在を見わける目的で，u' と w'についてのクロススペクトルを各ケースごとに求めた。石んを水中に入れて風波を消し，造波装置で起した長周期波だけのケースでは，波の各位置ごとに風速を平均することにより，波により誘起された速度変動成分が求められた。波高が 1.1cm と小さいときには，波により誘起されたレイノルズ応力は波の峯のすぐ上では正の値をとるが，高さと共にすぐ消失してしまうことがわかった。しかしながら波高が 6.0 または 7.0cm と大きいときには，波の峯の上の測定しうる最低の高さ（そこでは正になるようであるが）を除いたほとんどの高さで，はっきりと負の値をもっていた。風波だけのケースにおいては，波のすぐ上ではかなりの波によって誘起された速度変動成分があるが，それらはほとんど 90° 近い位相差をもっていて，cospectra への，すなわちレイノルズ応力への寄与はあまり大きくなかった。それでも冬期の実験結果では，負の応力が多少ある傾向が見られた。$-\overline{u'w'}$ の測定値には，定量的にも定性的にも季節ごとの差が存在したけれども，夏以外の季節にえられた測定結果からは，波のすぐ上の少しの高さで乱れのレイノルズ応力がほぼ一定に近いことがわかった。そしてそこでの値は，風速分布の水面に一番近い部分に対数法則をあてはめて求めた表面セン断力とだいたい一致した。石けんを使わず，したがって卓越した長周期波と小さな風波が共存する第3のケースでは，波によるレイノルズ応力は季節には関係なく，明らかに負の値のみを示し，また第1のケースとはやや対照的に，波のすぐ上の高さにおいても乱流変動成分の方がはるかに強力であった。

* 水工部 高潮津波研究室長
** 水工部 水理研究室

CONTENTS

Synopsis 3

1. Introduction 7

2. Experimental Equipment and Procedure 8

2.1 General Description of Experiments 8

2.2 Hot-Wire Operation 10

2.3 Velocity Measurement 11

3. Results and Discussions 13

3.1 The Cases of Clear Long Waves 13

3.2 The Cases of Wind Waves Only 20

3.3 The Cases of Composite Long Waves 29

4. Conclusions 32

References 33

List of Symbols 35

Appendix 37

1. Introduction

It is relatively recent years that the turbulent structures of wind over water waves were given attention in connection with the wave generation problem. Before the late 1950's the studies of wind in this context were conducted mainly in relation to the 'sheltering hypothesis' by Jeffreys (1924, 1925). Santon, Marshall & Houghton (1932) and Motzfeld (1937), respectively, made the measurements of air flow, especially the static pressure distribution, over the smooth solid wavy surface placed in a wind tunnel. Their results indicated that the pressure differences over those solid wave models are an order of magnitude smaller than the differences required by Jeffreys to account for the growth rate of observed waves. Although those results lowered the appraisal of the 'sheltering hypothesis' and led to a search for alternatives, these experiments were in fact almost irrelevant to the wave generation problem (Phillips, 1966).

In the late 1950's two wave generation theories were proposed by Phillips (1957) and Miles (1957), respectively. The former brought the turbulent character of wind into relief distinctly in relation to the wave generation, and the latter introduced the interaction between wind and waves in the inviscid wave generation theory. Miles (1957) discovered that a Reynolds stress is generated by the wave-induced air motion at the 'critical layer' where the wave speed equals the wind speed. This stress is then supported by the wave-induced velocity fluctuations in the air flow below the 'critical layer', and continually transfers momentum to the waves.

Since then not a few relevant experimental results have been published, mostly in favor of the inviscid theory by Miles for several years. Later on, however, it was found by Snyder & Cox (1966) and also Barnett & Wilkerson (1967) that the growth rate of waves observed in ocean is much greater than that predicted by the inviscid theory. In the meantime generalizing the inviscid theory, Phillips (1966) presented the detailed analytical discussions concerning the momentum transfer mechanism by the wave-induced turbulent air motion. Miles (1967) brought forward a conjecture that the significance of wave-induced perturbations in the turbulent Reynolds stresses for momentum transfer from wind to waves must increase with an appropriate scale parameter which is substantially larger in the field observations than the laboratory experiments. Miles also made it clear that the more detailed experimental data of those turbulent Reynolds stresses is a prerequisite to the further theoretical progress. Although Stewart (1967) submitted some doubts about the whole concept of Miles (1957) and alternatively proposed new ideas involving the effect of the turbulence in wind and of different flow configurations from that of Miles, the validity of those ideas could not be checked either for lack of the relevant wind data.

Even part from the connection with the wave generation problem, it is required from the engineering point of view to study the turbulent structures of wind over waves, especially in relation to the applicability of the so called log-law. That is, although the log-law has been well established for the wind profiles over the fixed rough surface, it will not be unfair to say that the relation has not yet been confirmed critically for the wind over the water waves. This is mainly because there is no means to measure the surface shear stress τ_0 so accurately as to be able to check the validity of the log-low. Nevertheless the log-

law has often been used in order to obtain the friction velocity u_* from the wind profiles, occasionally in conflicting ways.

The measurements of wind velocity spectra and Reynold stresses over the sea were made by Pond *et al.* (1963, 1966), Smith (1967) and Weiler & Burling (1967). Although these results were almost irrelevant to the wave generation problem, they contributed to shed light on the turbulent structures of wind up to several meters above the ocean waves.

In the laboratory Kato & Sano (1969) conducted the measurements of the wind velocity fluctuations over waves (with and without mechanically generated waves) by the use of a hot-wire and the digital method, and found that although there do exist the wave-induced velocity fluctuations in the degree in accordance with the wave conditions and the height above the wave crests, the turbulent fluctuations are predominant in general.

Recently Kendall (1970) measured the wind velocity fluctuations over the wavy wall made of a smooth neoprene rubber sheet which progressed upwind or down at controlled speed, and obtained the various wave-induced double correlation terms relevant to the wave generation theory. The results indicated that the waves strongly modulate the turbulent structure. The measurements of the horizontal and vertical velocity fluctuations over water waves were also made by Shemdin & Lai (1970) with and without mechanically generated waves in a wind-wave channel by the use of hot-film anemometers.

In this report we describe the primary results of an experimental study on the turbulent structure of wind and the wave-induced air motions over the three kind of waves in a wind-wave tunnel by the use of an X-array hot-wire system and the digital method similar to that described in the previous report (Kato & Sano, 1969).

2. Experimental Equipment and Procedure

2.1 General Description of Experiments

The present experiments were conducted in the same wind-wave tunnel as had been used in the previous experiments. The general sketch of the facility is again shown in Fig. 1. The uniform test section is 150 cm wide, 130 cm high and 2850 cm long. The side walls and most of the ceiling consist of glass plates. The enlarged part is situated on the leeward of the test section as seen in Fig. 1.

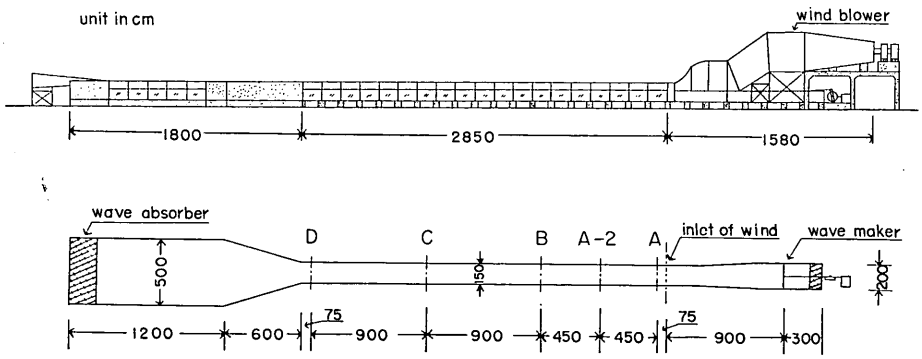

Fig. 1. Wind-Wave Tunnel

At the leeward end of this part, wind is diffused and surface waves are dissipated by a slope of pebbles and stainless steel turnings. At the wind ward end of the waterway, a mechanical wave generator of piston type is equipped to generate regular waves of relatively long period. On the windward side of the test section is situated a wind blower, where wind is generated by an axial fan driven by a 50 KW variable-speed motor. Large scale turbulence and rotation of air flow caused by the fan are eliminated through guide vanes, a fine mesh screen and honeycombs. After passing the contraction section, air flow is supplied onto the water surface at the inlet section (shown in Fig. 1) by means of an adjustable-height transition plate of 3 m length which is hinged at the windward end. At the Section A, 75 cm leeward of the inlet, the wind speed distribution is quite uniform both vertically and horizontally and the turbulence level $\sqrt{\overline{u'^2}}/U$ (u'= streamwise velocity fluctuations, U=mean wind speed) is nearly 0.4%.

In the present study, the measurements were made of wind velocity fluctuations at the Section C of 18.75 m fetch under the several conditions of waves and wind speeds. Usually the number of revolution of blower's fan per minute (rpm) is effectively used for setting up a particular wind speed by adjusting and monitorring it to the order of 0.1 rpm throughout a particular run by means of an electric tachometer. Mainly we used the wind speeds for rpm 100, 200 and 300, respectively. The corresponding mean wind speeds at A section were nearly 2.6, 5.6 and 8.2 m/sec, respectively, and the maximum wind speeds at the measurement station (C section) were roughly 3.1, 6.3 and 9.5 m/sec, respectively, slightly depending on the water surface conditions. The daily differences of the real (measured) maximum wind speed at C section in the same case for the same rpm were less than about 1%.

The measurements were performed under the three different wave conditions; that is, (i) the case of wind waves only, where the wind was blown over the clean still water, (ii) the case of mechanically generated long waves with height of 5.7 cm and period of 1.60 seconds, where the wind waves naturally generated coexisted, and (iii) the case of clear long waves with period of 1.60 seconds, where the suitable amount of soap was applied into water to eliminate wind waves completely and the water surface undulations were nearly sinusoidal. We will call the second condition the case of 'composite long waves' in this report although the term of 'superposed long waves' was used in the previous one. The wave heights of 'clear long waves' used were 1.14, 5.98 and 7.03 cm. The combinations of those winds and waves will be shown later.

A digital data recorder (DATAC-2000, Iwasaki Commun. Instr. Co.) was used for recording the output voltages from the hot-wire systems and the capacitance wave meter. The recorder has three input channels now. After being pre-amplified by the precision DC-amplifiers, if necessary, the input analog data are converted into digital quantities and are recorded on a magnetic tape of 1/2 inch width in a format fitted to the digital computer. The significant figures of the A-D converter are three ($-999 \sim +999$) and the converting time is less than 150 μ seconds. The sampling time intervals available are from 1/45 to 1/1440 second for one channel use. The quasi-simultaneous sampling is also possible, where the time lag between the successive channels is 150 μ seconds. This type of sampling was used for the multi-channel recording throughout the experiments.

2.2 Hot-wire Operation

Horizontal (streamwise) and vertical wind velocity fluctuations were measured by means of an X-wire probe and two suits of constant-temperature hot-wire anemometer and linearizer system with a high frequency response, reported by the manifacturer (Nihon Kagaku Kogyo Co.), of 0~50 KHz. The X-wire element consists of two tungsten wire of 5 $\mu\phi$ and 1 mm length fixed crossing each other at the angle of 90°. The element is attached to the support of 8 mmϕ in such a way that each hot-wire makes the angle of ±45° to the horizontal direction in a vertical plane parallel to the wind direction as shown in Fig. 2.

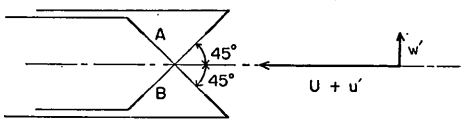

Fig. 2. Orientation of an X-Wire Element

The relation between the output voltage from the anemometer E and the normal wind speed to a hot-wire V, for a particular operating condition with constant surrounding temperature, is expressed to a good approximation as

$$E^2=E_0^2+a_1V^{1/2}\,, \tag{1}$$

where E_0 and a_1 are constants. We feed this voltage E to the linearizer to obtain the output voltage M linearly proportional to V such as

$$M=KV\,. \tag{2}$$

The coefficients K_A and K_B for each wire were obtained from the calibration carried out just before the each day measurements by placing an X-wire and a pitot static tube side by side at the center position (z=40 cm) of the tunnel core portion at C section where the turbulence level was fairly low as will be shown later. For four or five different wind speeds, the mean wind speed $\bar{V}$ ($=U/\sqrt{2}$) were measured by using the pitot static tube, while the linearizer output voltages were recorded with the digital data recorder described above to obtain the mean voltages $\bar{M}_A$, $\bar{M}_B$. The calibration curves thus obtained, one of which is shown in Fig. 3, were satisfactorily linear in general.

The total voltages, X and Y, from the X-wire system described above (X corresponding to a wire A in Fig. 2) are related to the wind velocity components by

$$\left.\begin{aligned} X&=\frac{1}{\alpha'\sqrt{2}}\left[U+(u'+w')+\frac{w'^2}{U}-\frac{w'^2(u'+w')}{U^2}+\cdots\right],\\ Y&=\frac{1}{\beta'\sqrt{2}}\left[U+(u'-w')+\frac{w'^2}{U}-\frac{w'^2(u'-w')}{U^2}+\cdots\right], \end{aligned}\right\} \tag{3}$$

where u', w' are the total streamwise and vertical velocity fluctuations, respectively, U the mean velocity, and α', β' are the constants determined from the calibration ($\alpha'=K_A$ and $\beta'=K_B$). There-

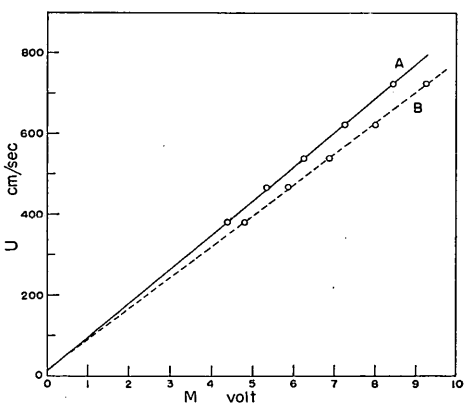

Fig. 3. An example of the X-Wire Calibration Curves

fore the first order fluctuating voltage components, X' and Y' are given, respectively, by

$$\left.\begin{aligned} \alpha' X' &= \frac{1}{\sqrt{2}}(u'+w') , \\ \beta' Y' &= \frac{1}{\sqrt{2}}(u'-w') . \end{aligned}\right\} \tag{4}$$

By putting $\alpha'/\sqrt{2}=\alpha$, $\beta'/\sqrt{2}=\beta$, u' and w' are obtained as follows:

$$\left.\begin{aligned} u' &= \alpha X'+\beta Y' , \\ w' &= \alpha X'-\beta Y' . \end{aligned}\right\} \tag{5}$$

Usually u' and w' may be obtained by the analog method from (5); if the sensitivities of two linearizers are adjusted to produce the same conversion coefficients such as $\alpha=\beta$, then the adding and subtracting circuits give u' and w', respectively. In the present experiments, however, the instantaneous total voltages, X and Y, were recorded in the digital form at the small time interval Δt by means of the digital data recorder, and u' and w' were evaluated at the interval Δt from the relation (5) by using a computer. This digital method enabled us not only to save time in setting the instruments but also to apply the precise conversion coefficients α and β.

2.3 Velocity Measurement

At the wind field over water waves, the total velocity fluctuations u', w' are resolved as follows:

$$\left.\begin{aligned} u' &= \tilde{u}+u_t' , \\ w' &= \tilde{w}+w_t' , \end{aligned}\right\} \tag{6}$$

where $\tilde{u}$, $\tilde{w}$ are the wave induced periodic components and u_t', w_t' the turbulent components. Since the measurements were made in the middle vertical plane of the tunnel width, the air flow there may be assumed as two-dimensional. In the present study we measured the wave induced components as the phase-average values with respect to time, not the mean values with respect to the transverse coordinate (cf. Phillips, 1966, p. 90). That is, for the case of clear long waves in our experiments,

$$\left.\begin{aligned} \tilde{u}(t_\varepsilon) &= \langle u' \rangle_\varepsilon = \frac{1}{N}\sum_{j=1}^{N} u'(t_\varepsilon + jT_p) , \\ \tilde{w}(t_\varepsilon) &= \langle w' \rangle_\varepsilon = \frac{1}{N}\sum_{j=1}^{N} w'(t_\varepsilon + jT_p) , \end{aligned}\right\} \tag{7}$$

where t_ε denotes a time corresponding to a particular wave phase, $\langle\ \rangle_\varepsilon$ the time average with respect to a particular wave phase ε and T_p the wave period. If $\langle\ \rangle$ is simply used in the following, a particular phase is related implicitly in the case of clear long waves. For the case of wind waves only, however, such averaging was not possible and only the total power of the wave induced components was roughly estimated.

In the present study we made use of the cross spectral analysis with respect to u' and w' in the digital way extensively, because we thought this was the only means to detect the wave-induced velocity components, especially the wave-induced Reynolds stresses in the cases of wind waves only (u'- and w'-spectra were obtained as by-products). The computation procedures used were the same as those in the previous report (Kato & Sano, 1969) and of general type. We usually took $\Delta t=1/30$ second in these computations to obtain the frequency resolution $\Delta f=0.1$ Hz with a maximum lag of 150, yielding the holding frequency $f_N=15$ Hz. There was naturally the same problems of aliasing as discussed in some detail for the computations of auto-spectra in the previous report (Kato & Sano (1969), see also Blackman & Tukey (1958)). To eliminate the aliased power, we occasionally used a simple numerical filter (3-point sliding mean) as follows:

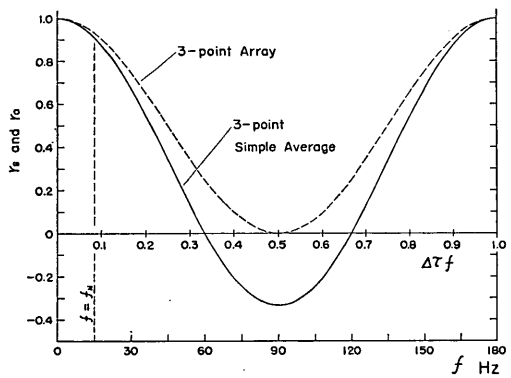

Fig. 4. Frequency Response of the 3-Point Sliding Mean and Array

$$y_i=\frac{1}{3}(x_{i-1}+x_i+x_{i+1})\,, \quad (8)$$

where x_i is input data and y_i output of i-th. If the original sampling time interval is $\Delta\tau$, the attenuation factor r_s at frequency f is given by

$$r_s(f)=\frac{1}{3}(1+2\cos 2\pi f\Delta\tau)\,. \quad (9)$$

The relation (9) is shown in Fig. 4, together with that for a 3-point array:

$$\left.\begin{aligned} &y_i=0.25x_{i-1}+0.5x_i+0.25x_{i+1}\,,\\ &r_a(f)=\frac{1}{2}(1+\cos 2\pi f\Delta\tau)\,. \end{aligned}\right\} \quad (10)$$

It is found from Fig. 4 (where $\Delta t=6\Delta\tau$) that the filter not only eliminates the aliased power but also cut down the required components at the frequencies lower than f_N. The results obtained by this filter (8) with $\Delta t=1/180$ second are distinguished by M attached to the run-number in the later figures, like Y3312-M.

The simpler computation procedures were also used to obtain just $\overline{u'w'}$, $\overline{u'^2}$ and $\overline{w'^2}$ for all cases, and the following relation was also useful:

$$\overline{u'w'}=\alpha^2[\overline{X^2}-(\bar{X})^2]-\beta^2[\overline{Y^2}-(\bar{Y})^2]\,, \quad (11)$$

where — denotes overall time average. In the case of clear long waves, we measured $\tilde{u}$ ($=\langle u'\rangle$, $\tilde{w}$, $\langle u'^2\rangle$, $\langle w'^2\rangle$ and $\langle u'w'\rangle$ by applying the procedure shown in (7), from which further $\tilde{u}\tilde{w}$, $\langle u_t'^2\rangle$, $\langle w_t'^2\rangle$ and $\langle u_t'w_t'\rangle$ were estimated by using the following relations:

$$\left.\begin{aligned} &\langle u_t'^2\rangle=\langle u'^2\rangle-(\tilde{u})^2\,,\\ &\langle w_t'^2\rangle=\langle w'^2\rangle-(\tilde{w})^2\,,\\ &\langle u_t'w_t'\rangle=\langle u'w'\rangle-\tilde{u}\cdot\tilde{w}\,. \end{aligned}\right\} \quad (12)$$

In these cases we took special care for the period of wave generator to be exactly 1.60 seconds; practically the deviation of total time corresponding to 300 wave periods was reduced to less than 0.2 second by using a stopwatch. For the cases of the wave height $H=6.0$ cm, we recorded the water surface undulations at C section simultaneously with the wind velocity data by means of a capacitance wave gauge placed near one side wall of the wind-wave tunnel. These wave data indicated that there existed a small shift of the wave period. Usually the sampling time interval was $\Delta t=1/30$ and the total data number for a single number for a single computation $N=6000$. The position of wave crest, which should appear at every 48 data, shifted in the worst case by 6 or 7 after 124 waves (=5952 data). It was found later that the mean values simply evaluated with respect to every 48 data gave fairly good results, even if the phase shift of this much existed. However, in the final computations of the relations such as (12) for the cases of $H=6.0$ cm we made corrections so that the computed and real phase positions might not drift apart by more than one data. In the cases of $H=1.14$ cm such a correction was not made because a slight level of the noise voltages from the capacitance bridge somewhat obscured the real crest positions.

3. Results and Discussion

3.1 The Cases of Clear Long Waves

In these cases the waves with a single period of 1.60 seconds were generated by a wave generator, the wind waves being suppressed completely by applying soap into water. The wave heights used in the experiment were mainly $H=6.0$ cm and $H=1.14$ cm, and supplementally $H=7.0$ cm. The wind speed used were those established at rpm 200 and rpm 100. The corresponding mean wind velocity profiles in the cases of $H=6.0$ cm and $H=1.14$ cm are shown in Figs. A-1 and A-2 in the Appendix. Note that a critical layer, where $U=c$ ($\fallingdotseq$192 cm/sec), appeared at the height of $z=3$ cm in the case of $H=1.14$ & rpm 100, while in the other cases all measurements were made far above the critical layers. All experiments in these cases were conducted at the room temperature of 15.0~19.0°C and that of water 14.0~15.5°C in November, and it is likely that the hot-wire results were not effected seriously by the seasonal difference, whatever the cause may be, which will be discussed later.

The u'- and w'-spectra at a few heights in each case are shown in Figs. A-3 to A-6 to observe the relative magnitudes of wave-induced components which appear near the frequency of clear long waves, $f_L=0.625$ Hz. It is found from Figs. A-5 and A-6 that in the cases of $H=1.14$ cm strong wave-induced powers exist in u'-spectra rather than w' at the lowest height ($z=1.2$ or 1.5 cm) above the wave crests and that they are reduced rapidly with increasing height. On the other hand, the dominant powers induced by waves appear in w' rather than u' in the case of $H=6.0$ & rpm 200 and in both u' and w' in the case of $H=6.0$ & rpm 100 at the lowest height ($z=4.0$ cm) as seen from Figs. A-3-(a) and A-4-(a), respectively. It is further seen that these wave-induced powers do not decrease remarkably with height, which was already pointed out in the previous report (Kato & Sano, 1969).

The variations of co- and quad-spectra with height in each case mentioned above are shown in Figs. 5~8, and the corresponding coherences $\hat{\gamma}^2$ are shown

in Figs. A-7~A-10 in Appendix. The whole results at $z=4$ cm in the case of $H=7.0$ cm & rpm 200 are shown in Fig. 9. The digital computations were performed with $\Delta t=1/30$ second, $N=6000$ and maximum lag $h=150$. The spectral densities for $f>7$ Hz are omitted in these figures because no significant power existed there. The remarkable variations of the spectral density around $f\fallingdotseq 0.6$ Hz are considered to correspond to the wave-induced components; the projection (or depression) of co-spectral density there indicates the existence of the positive (or negative) wave-induced Reynolds stress. Since $-\overline{u'w'}$ is related to the co-spectral density by

$$-\overline{u'w'}=-\int_0^\infty C_{u'w'}(f)df\,, \tag{13}$$

it is expected that the area, which is the projecting (or depressing) part and a line connecting the both side showing no wave-induced power, is nearly equal to to the value of $-\tilde{u}\tilde{w}$ (see Fig. 10).

On the other hand, the phase averaging described earlier (p. 11) yielded $\tilde{u}$ and $\tilde{w}$, from which $-\tilde{u}\tilde{w}$ were evaluated directly. $-\tilde{u}\tilde{w}$ thus obtained are shown

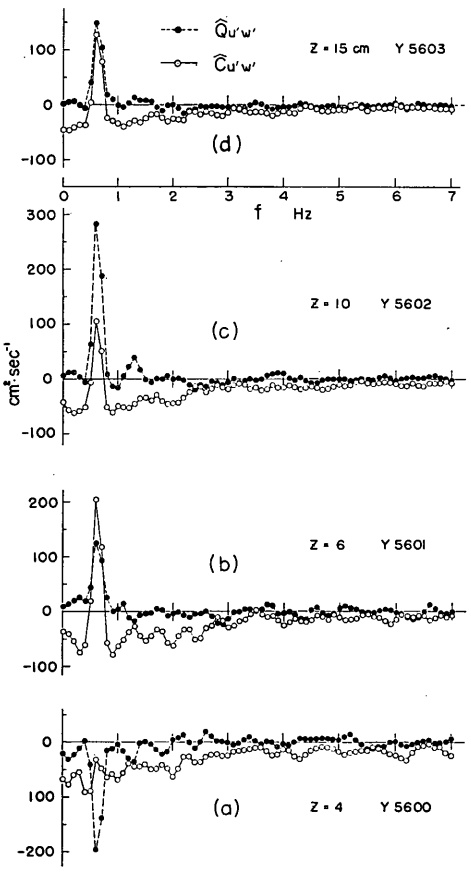

Fig. 5. Co- and Quad-Spectra in the cases of clear long waves; rpm 200, $H=6.0$ cm

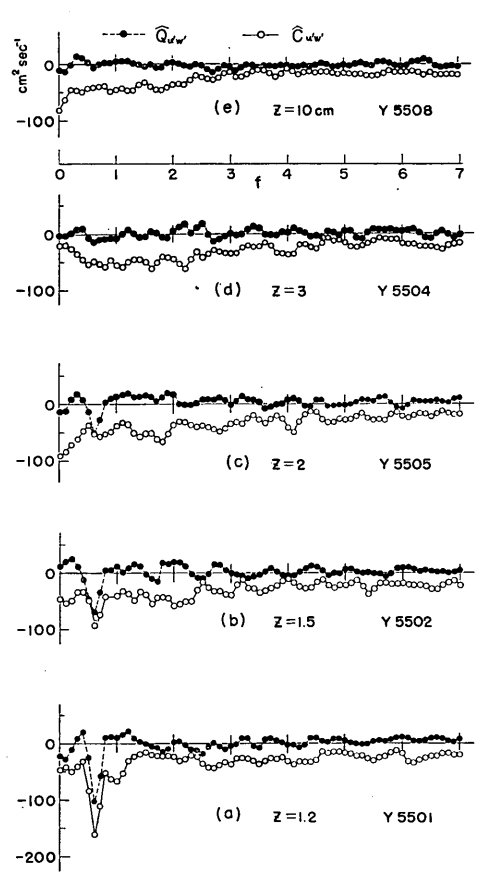

Fig. 6. Co- and Quad-Spectra in the cases of clear long waves; rpm 200, $H=1.14$ cm

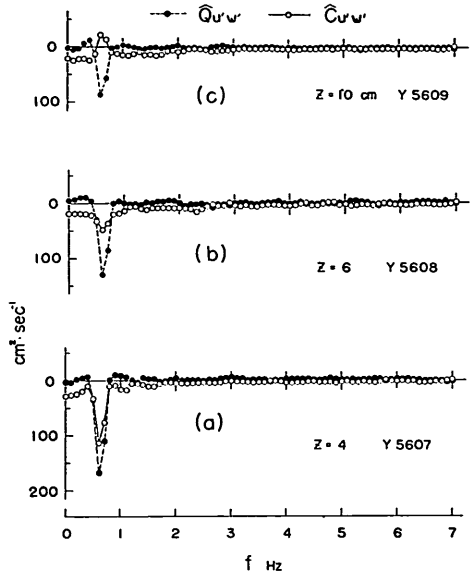

Fig. 7. Co- and Quad-Spectra in the cases of clear long waves; rpm 100, H=6.0 cm

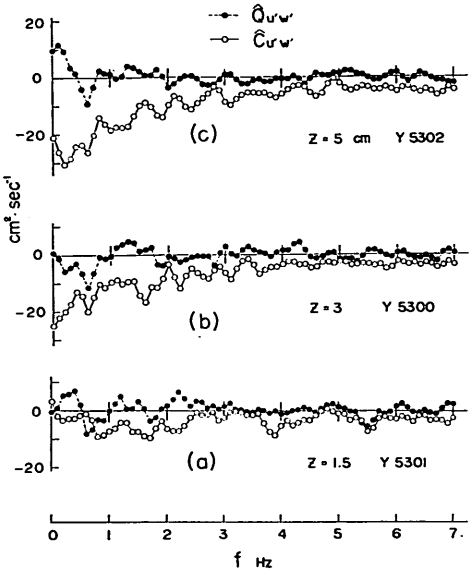

Fig. 8. Co- and Quad-Spectra in the cases of clear long waves; rpm 100, H=1.14 cm

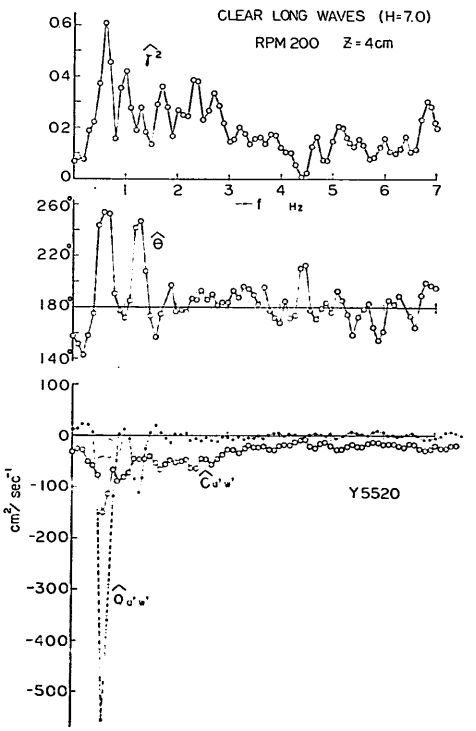

Fig. 9. Cross Spectrum in the case of clear long waves; rpm 200, H=7.0 cm, z= 4 cm

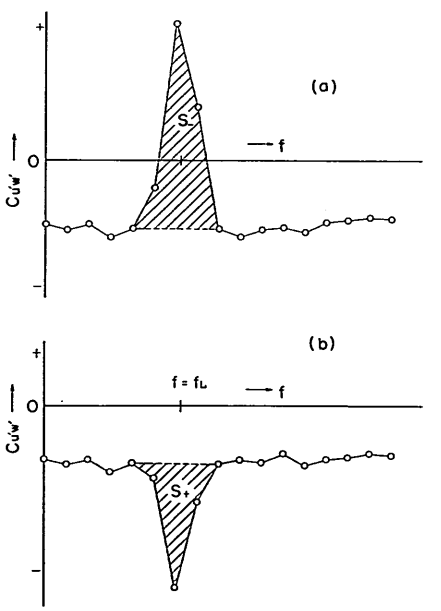

Fig. 10. Graphical Estimation of the Wave-Induced Reynolds stresses: Areas S_- in (a) and S_+ in (b) are nearly equal to the negative and positive stresses, respectively

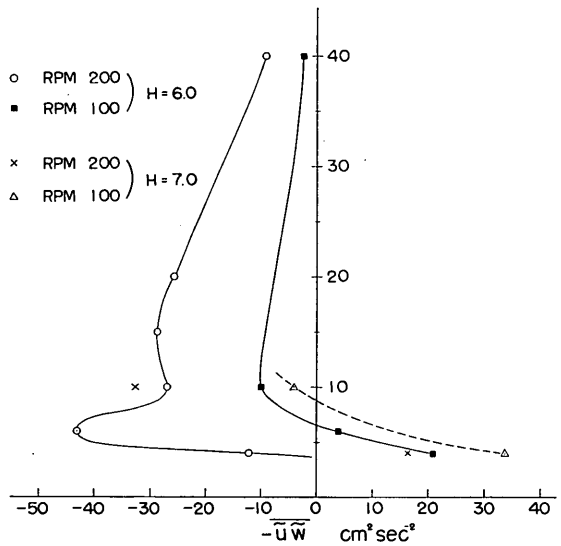

Fig. 11. Wave-Induced Reynolds Stresses in the cases of clear long waves; rpm 200 & 100, H=6.0 & 7.0 cm

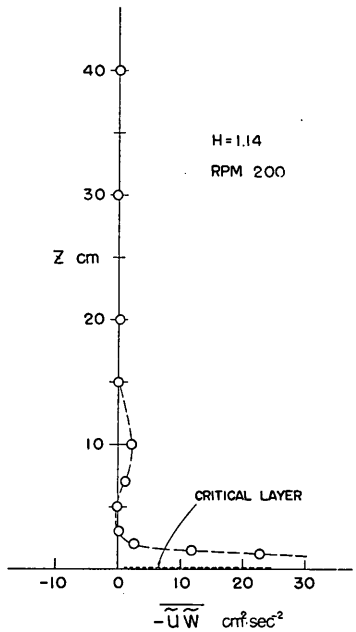

Fig. 12. Wave-Induced Reynolds Stresses in the case of clear long waves; rpm 200, H= 1.14 cm

in Figs. 11~13. The values of $-\overline{\tilde{u}\tilde{w}}$ estimated roughly from the variations of co-spectra in the way shown in Fig. 10 coincided with those from phase averaging very well (within 3%) for the cases of Figs. 6-a and 7-a and reasonably well (10~20%) for other cases with detectable wave-induced powers.

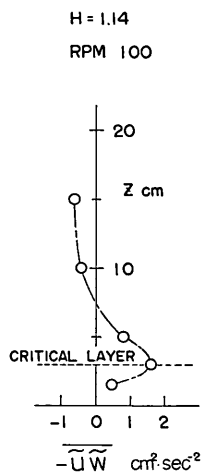

Fig. 13. Wave-Induced Reynolds Stresses in the case of clear long waves; rpm 100, H=1.14 cm

According to the inviscid theory by Miles (1957), the wave-induced Reynolds stress exists only below a critical layer; $\tilde{u}$ and $\tilde{w}$ at the height above the critical layer are just 90° out of phase, yielding $\overline{\tilde{u}\tilde{w}}=0$ there. Recently Hamada (1968) introduced the instability Reynolds stresses other from Miles theory which might exist near the water waves but above the critical layer, if the separation or sliding of air flow took place at the water surface. Hamada expected this would be an effective cause of the deviation of wind speed near the water surface in a wind-wave tunnel from the so-called log-law.

The wave-induced Reynolds stresses measured in the cases of 'clear long waves' appeared in a fairly complicated way. The results in the case of H=1.14 & rpm 100 may be less reliable because of their small values, but in other cases the wave-induced Reynolds stresses definitely existed above the critical layer. In the case of H=1.14 & rpm 200 (shown in Fig. 12), positive wave-

induced Reynolds stress appeared at the lowermost measurement height (z=1.2 cm) above the wave crests and they decreased very rapidly with z, becoming substantially to zero at z=3 cm, but no negative wave-induced Reynolds stress appeared. In the cases of H=6.0 or 7.0 cm (Fig. 11) the wave-induced Reynolds stresses had positive values or a strong tendency toward positive side at the lowermost measurement height, but they became definitely negative at a little larger height. These negative stresses remained until the height of z=40 cm although the absolute values decreased very slowly with z.

The appearance of negative wave-induced Reynolds stress in the cases with larger waves was rather unexpected result, and the authors suspect that this implys a peculiarity of the experiment conducted in a wind-wave tunnel fundamentally different from the phenomena in the open field conditions. The similar results were also obtained by Kendall (1970) in the measurement of $-\overline{\tilde{u}\tilde{w}}$ above the mechanically generated wave train in a sheet of smooth neoprene rubber. On theother hand, Shemdin & Lai (1970) reported nearly contrary results with respect to the signs of the stress, which will be discussed later.

For the cases of H=6.0 cm (both rpm 200 and rpm 100), we also made an attempt to estimate the double correlation terms $\langle u_t'^2\rangle$, $\langle w_t'^2\rangle$, and $\langle u_t'w_t'\rangle$, by the method described earlier (p. 12), which were originally introduced by Phillips (1966, p. 97) to appear into the vorticity equation governing the wave-induced turbulent air motion. Those quantities together with $\tilde{u}$, $\tilde{w}$ and $\tilde{u}\tilde{w}$ are shown in Figs. 14~18. A direction entitled 'down wind direction' shown in each figure indicates which of the two phase positions taken on the abscissa was situated leeward. There exist considerable scatter especially in $-\langle u_t'w_t'\rangle$, which is probably attributed to the lack of the total wave number for averaging. The vertical distributions of the turbulent Reynolds stress, $-\overline{u_t'w_t'}$, in the cases of H=1.14 cm, where the measurement could be made relatively close to the mean water surface, are shown in Fig. 19. For the case of rpm 200 the distribution is similar to those measured in the boundary layer on the fixed wall (e.g. Hinze 1959, p. 491), and the stress tends to be constant at the heights lower than about 2.5 cm. On the other hand, for the case of rpm 100 $-\overline{u_t'w_t'}$ again decreases to-

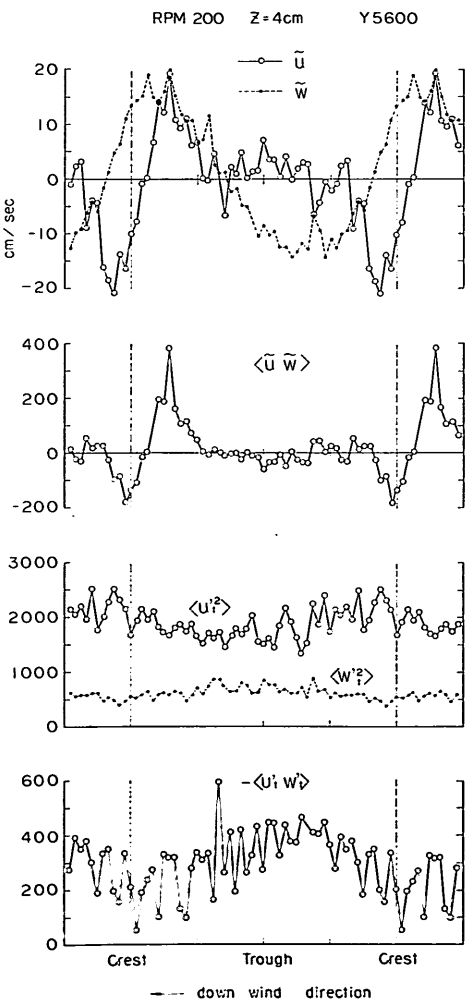

Fig. 14. $\tilde{u}$, $\tilde{w}$, $\langle\tilde{u}\tilde{w}\rangle$, $\langle u_t'^2\rangle$, $\langle w_t'^2\rangle$ and $-\langle u_t'w_t'\rangle$ in the case of clear long waves; rpm 200, H=6.0 cm, z=4 cm

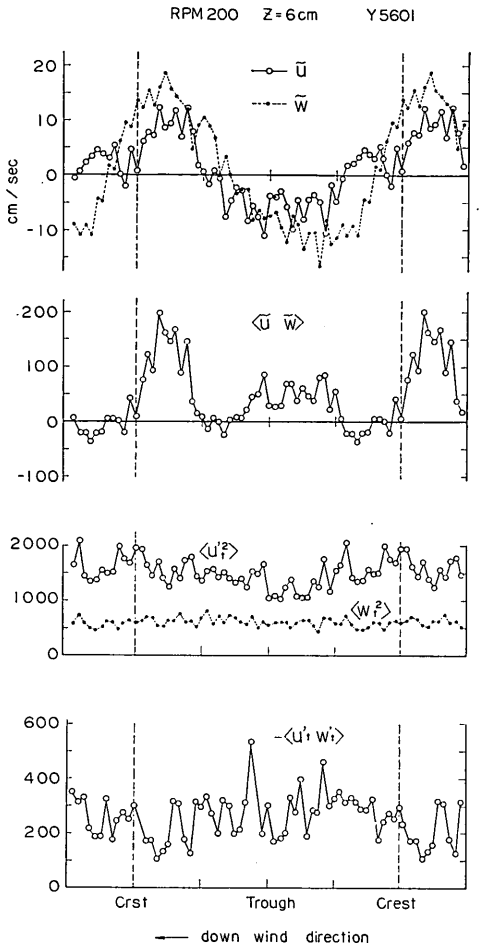

Fig. 15. $\bar{u}$, $\bar{w}$, $\langle\tilde{u}\tilde{w}\rangle$, $\langle u_t'^2\rangle$, $\langle w_t'^2\rangle$ and $-\langle u_t'w_t'\rangle$ in the case of clear long waves; rpm 200, H=6.0 cm, z=6 cm

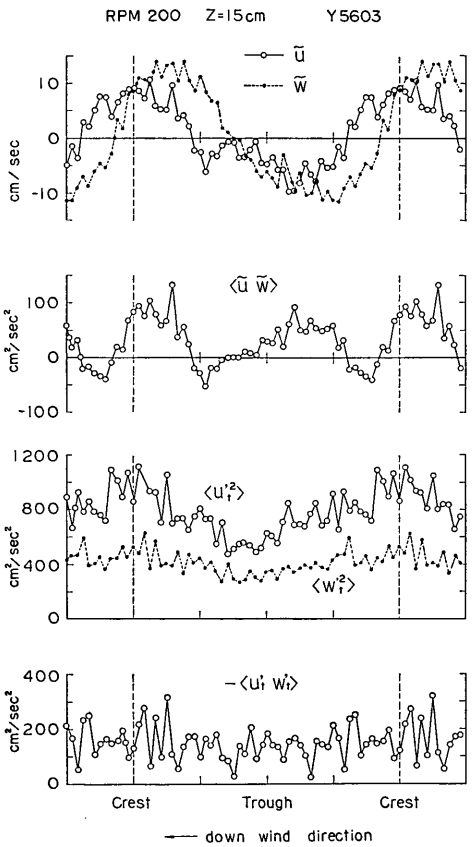

Fig. 16. $\bar{u}$, $\bar{w}$, $\langle\tilde{u}\tilde{w}\rangle$, $\langle u_t'^2\rangle$, $\langle w_t'^2\rangle$ and $-\langle u_t'w_t'\rangle$ in the case of clear long waves, rpm 200, H=6.0 cm, z=15 cm

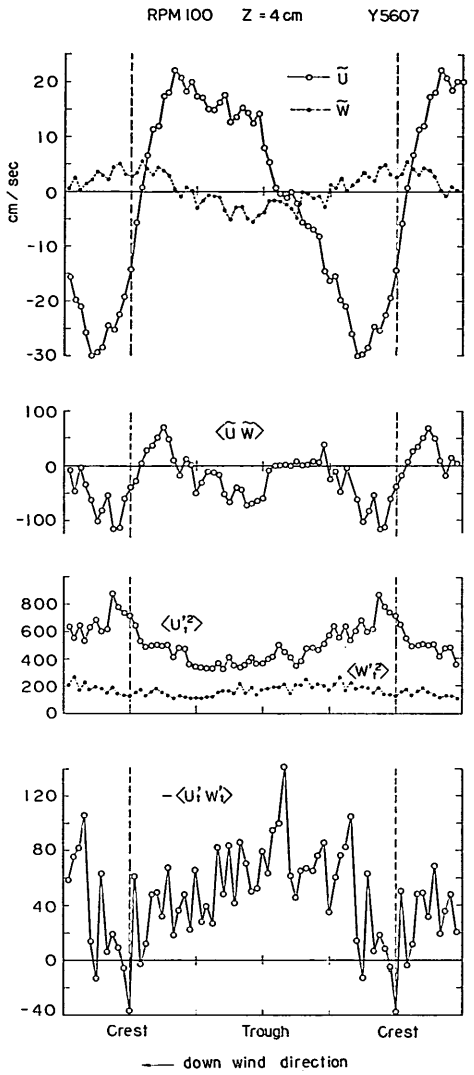

Fig. 17. $\tilde{u}$, $\tilde{w}$, $\langle\tilde{u}\tilde{w}\rangle$, $\langle u_t'^2\rangle$, $\langle w_t'^2\rangle$ and $-\langle u_t'w_t'\rangle$ in the case of clear long waves; rpm 100, H=6.0 cm, z=4 cm

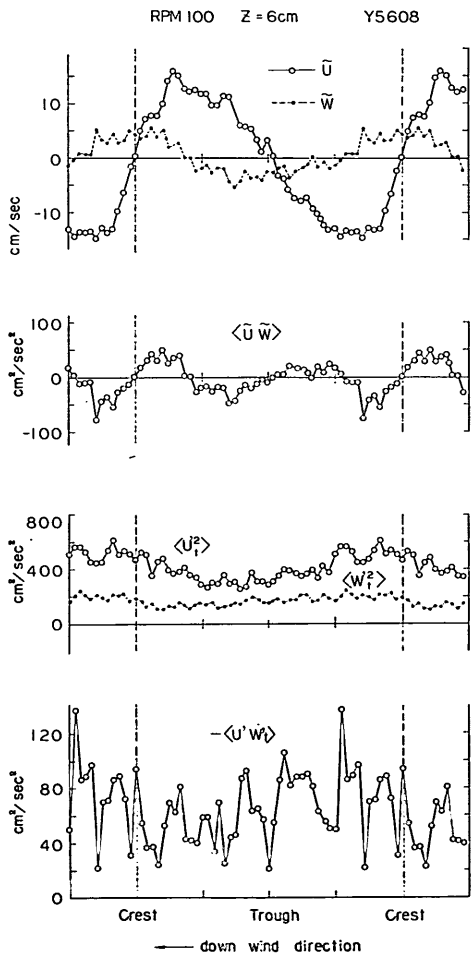

Fig. 18. $\tilde{u}$, $\tilde{w}$, $\langle\tilde{u}\tilde{w}\rangle$, $\langle u_t'^2\rangle$, $\langle w_t'^2\rangle$ and $-\langle u_t'w_t'\rangle$ in the case of clear long waves; rpm 100, H=6.0 cm, z=6 cm

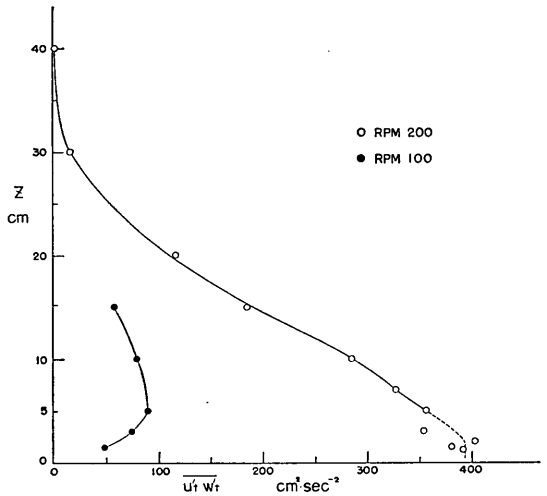

Fig. 19. Distributions of Turbulent Reynolds Stress in the cases of clear long waves; rpm 200 & 100, H=1.14 cm

ward the water surface at $z<5$ cm.

3.2 The Cases of Wind Waves Only

In this case the measurements at the wind speeds for rpm 300 were made twice and the measurements for rpm 200 were repeated several times throughout a year, because not only quantitative but also qualitative inconsistency was found in the values of total Reynolds stress obtained. As to the waves at the measurement station (C section) in these cases, the peak frequency f_p of the wave spectra and $H_{1/3}$ obtained from the total power of the spectra were $f_p \fallingdotseq 2.5$ Hz, $H_{1/3}=2.5$ cm for rpm 200 and $f_p \fallingdotseq 2.0$ Hz, $H_{1/3}=4.3$ cm for rpm 300.

The variations of the obtained $-\overline{u'w'}$ with height from the mean water surface are shown in Figs. 20 and 21. Fig. 20 for rpm 200 includes all the results in the measurements made at different seasons together with the experimental dates and room temperatures. At a glance, it is observed from the both figures that much scatter exists in the values of $-\overline{u'w'}$ near the water surface. Looking at carefully, it is found further that there is no doubt a tendency that the values of $-\overline{u'w'}$ near the water surface obtained at the season of high temperature (summer) are larger than those at low temperature (winter). Moreover, in the measurements at the time of high temperature the values of $-\overline{u'w'}$ increased monotonously with decreasing height, while at the lower temperature the maximum values turned up at a certain height z_m ($z_m \fallingdotseq 5\sim6$ cm for rpm 200 and $z_m \fallingdotseq 8\sim10$ cm for rpm 300) above the wave crests and below the height $-\overline{u'w'}$ decreased toward the water surface. It is seen from Fig. 20 that the lower the temperature was, the greater reduction in $-\overline{u'w'}$ took place at the lowermost measurement height. The variations of $\overline{u'^2}$ and $\overline{w'^2}$, which were measured simultaneously with $-\overline{u'w'}$ are shown in Figs. A-11 and A-12 in Appendix. Although there is considerable scatter in the values of $\overline{u'^2}$ and $\overline{w'^2}$ also, the seasonal trend can not be found so clearly as in $-\overline{u'w'}$. So far we have not been able to ascertain whether such a difference was caused simply by the instrumental errors or there is any trend in the natural wind properties.

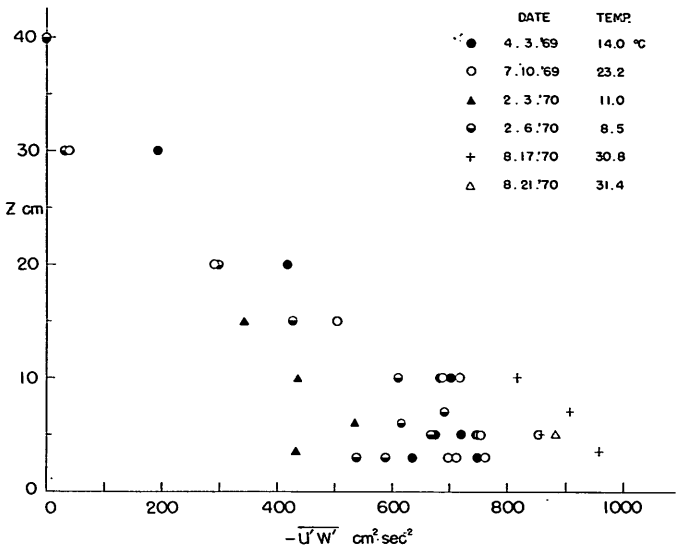

Fig. 20. Distributions of $-\overline{u'w'}$ in the cases of wind waves only; rpm 200

One thing we can suspect is that the difference of the vertical temperature distribution over the water surface may have resulted in such an inconsistency to some extent. We carried out the hot-wire calibration at the height of $z=40$ cm above the water surface as described previously, and the temperature of flowing air near the water surface is usually somewhat lower than that at the calibration height. This could, more or less, change the hot-wire calibration constants near the water surface. The influence of this change appears directly in the total output voltage, that is in the measurement of mean velocity. Since, however, this effect is considered to be much less influencial in the measurement

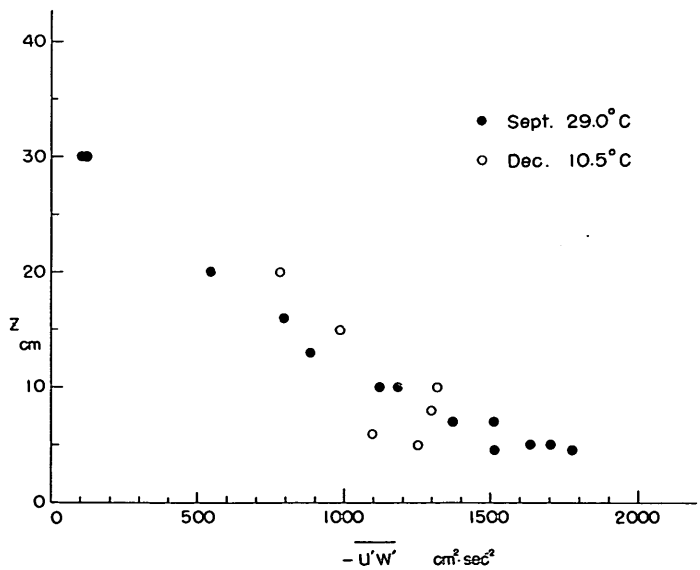

Fig. 21. Distributions of $-\overline{u'w'}$ in the cases of wind waves only; rpm 300

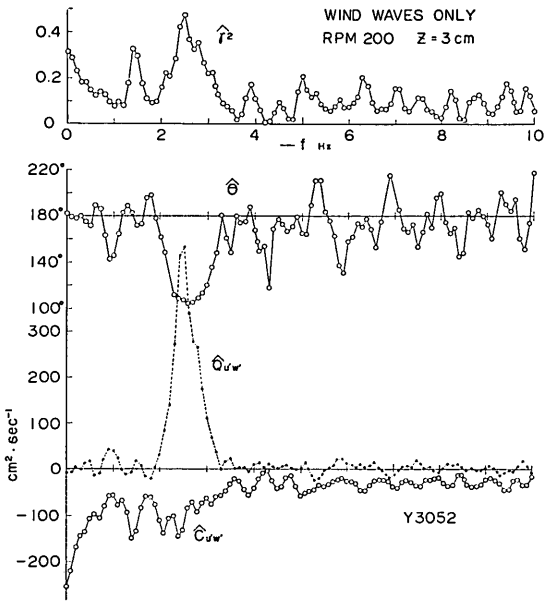

Fig. 22. *u'w'* Cross-Spectrum in the case of wind waves only; rpm 200, $z=3$ cm

of the fluctuating components, we have made no correction for this effect. The temperature difference ΔT between air (in the laboratory) and water is usually in the range of 4° to 5°C, but it increases up to about 6°C in summer and decreases down to about 2°C or less in winter (in autumn ΔT occationally becomes to nearly zero). When $\Delta T=6$°C in summer, the temperature difference of flowing air ΔT_1 between near the water surface and at $z=40$ cm could mount up to about 3°C for rpm 200 (cf. Kato & Takemura, 1966). When $\Delta T=2$°C or less in winter, ΔT_1 must be about 1°C or less. Such a degree of difference of ΔT_1, however, can hardly be considered to have produced the seasonal difference of the

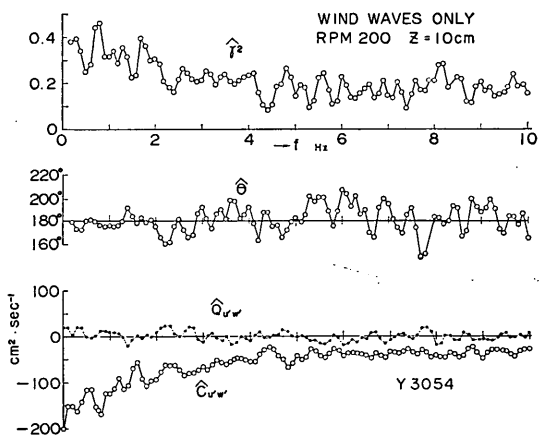

Fig. 23. *u'w'* Cross-Spectrum in the case of wind waves only; rpm 200, $z=10$ cm

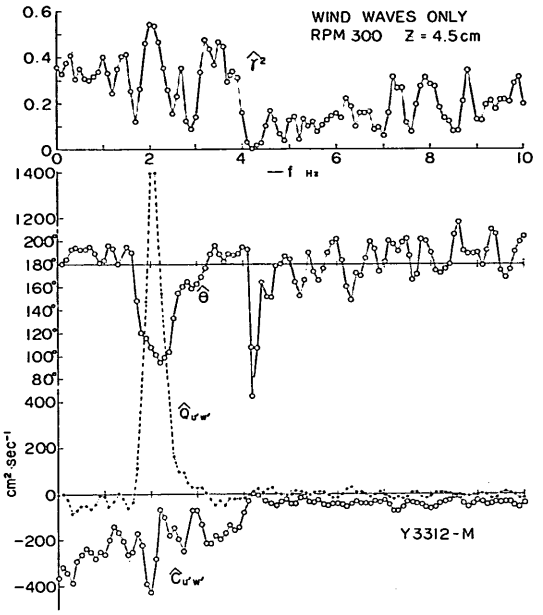

Fig. 24. $u'w'$ Cross-Spectrum in the case of wind waves only; rpm 300, z=4.5 cm

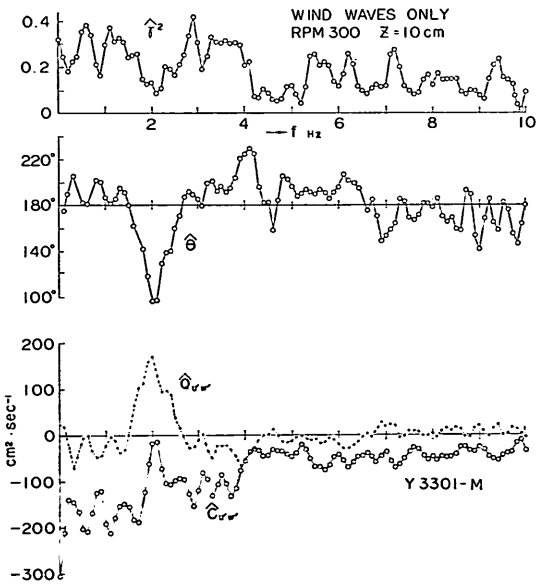

Fig. 25. $u'w'$ Cross-Spectrum in the case of wind waves only; rpm 300, z=10 cm

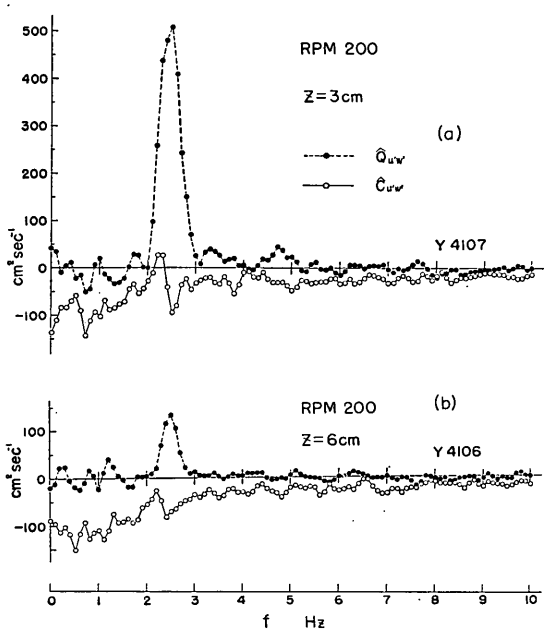

Fig. 26. Co- and Quad-Spectra in the cases of wind waves only; rpm 200; (a) z=3cm, (b) z=6cm

results so much as shown in Figs. 20 and 21.

As mentioned above the flowing air over the water surface was in more stable condition in summer than in winter. In a stably stratified shear flow the Reynolds stress is usually smaller than in a neutral flow. The seasonal difference of $-\overline{u'w'}$ found in the present experiment contradicts to the fact also.

Concerning the results of the cross spectra between u' and w', the effect of the different temperature (or season) was hardly observed except a weak tendency found in the variations of cospectra near the frequency f_p. Some of the whole cross spectral results, namely co- and quad-spectra $\hat{C}_{u'w'}$ and $\hat{Q}_{u'w'}$, phase

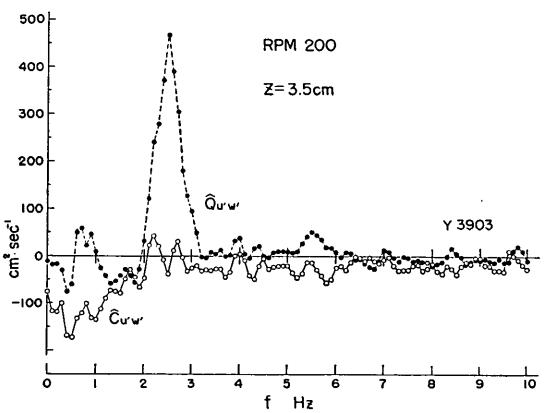

Fig. 27. Co- and Quad-Spectrum in the case of wind waves only; rpm 200, z=3.5cm

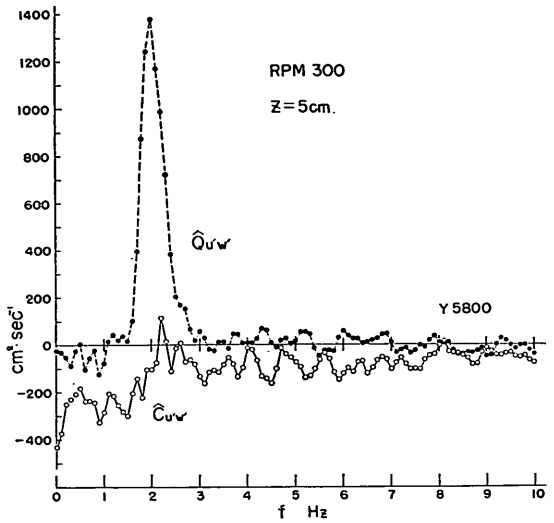

Fig. 28. Co- and Quad-Spectrum in the case of wind waves only; rpm 300, z=5 cm

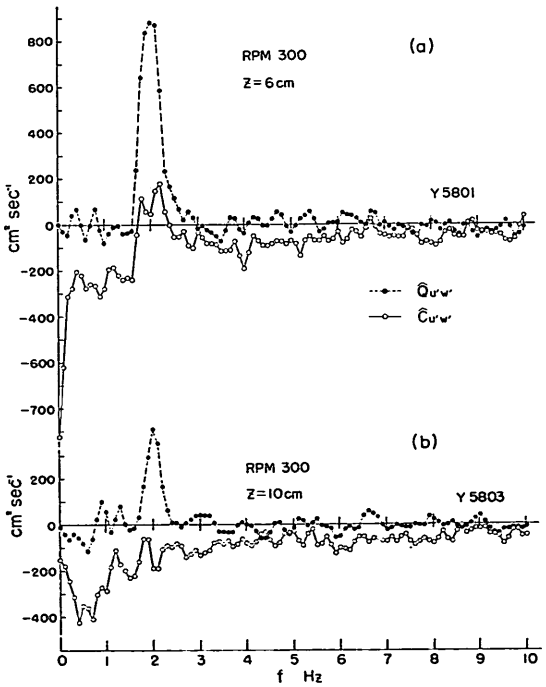

Fig. 29. Co- and Quad-Spectra in the cases of wind waves only; rpm 300; (a) z=6 cm, (b) z=10 cm

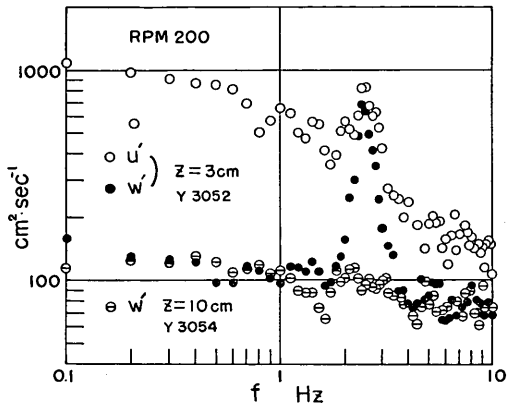

Fig. 30. u'- and w'-Spectra in the cases of wind waves only; rpm 200

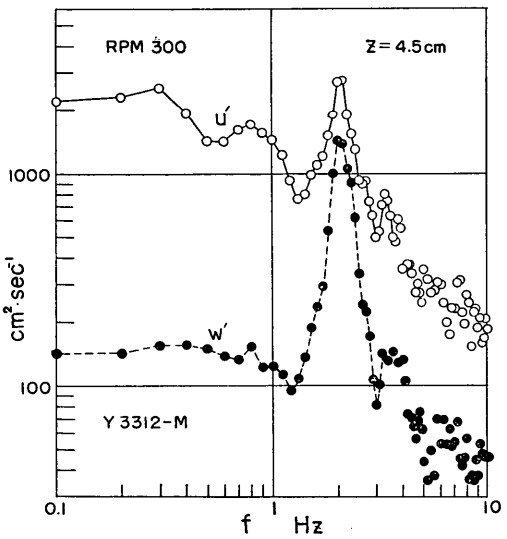

Fig. 31. u'- and w'-Spectrum in the case of wind waves only; rpm 300, z= 4.5 cm

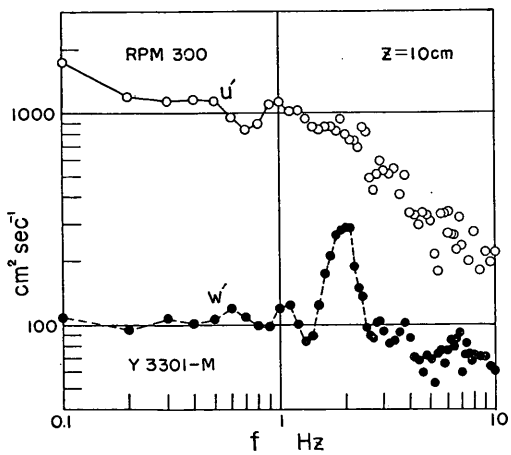

Fig. 32. u'- and w'-Spectrum in the case of wind waves only; rpm 300, z= 10 cm

angles $\hat{\theta}$ (which represents the phase lags of the w'-record relative to the u'-record) and coherences $\hat{\gamma}^2$, are shown in Figs. 22 and 23 for rpm 200 (at Temp.≒23°C in July) and in Figs. 24 and 25 for rpm 300 (at Temp.≒29°C in Sept.), which were obtained at the seasons of relatively high temperature as indicated in the parentheses above. The results of co- and quad-spectra, which were obtained at the winter season, are shown in Fig. 26-a, b (at Temp.=8.5°C) and Fig. 27 (Temp.≒11.5°C) for rpm 200 and in Figs. 28 and 29-a, b for rpm 300 (Temp.≒10.5°C). Examples of u'- and w'-spectra are shown in Figs. 30~32.

As seen from Figs. 30 and 31, there exist considerable wave-induced velocity fluctuations, which appear near the frequency f_p in the u'- and w'-spectra, at the lowermost measurement heights above the wave crests and the bulk of w'-power there consists of the wave-induced component. Figs. 22 and 24 indicate that these wave-induced u' and w' components are nearly 90° out of phase (u' component is leading) and that they do not make much contribution to the cospectra if any, although a strong peak appear near the frequency f_p in the quad-spectra. However, most of the cospectra at the small heights obtained in winter show signs of negative wave-induced Reynolds stress in the same way as illustrated in Fig. 10. For the case of rpm 300, shown in Figs. 28 and 29-a, the magnitudes of the negative stresses estimated by the graphical method of Fig. 10 are nearly as large as the magnitudes of the reduction in $-\overline{u'w'}$ near the water surface (see also Fig. 21). For the cases of rpm 200, the magnitudes of the negative stresses estimated in the same way seem to be a little smaller than those of the reduction in $-\overline{u'w'}$ near the water surface, and the reduction may be distributed in a wider frequency range. On the other hand, some of the $u'w'$-cospectra obtained at the summer season even show, in fact, slight indications of the positive wave-induced Reynolds stress. Such a typical example is presented in Fig. A-13 in Appendix, but note that this is the same experimental case as that shown in Figs. 24 and 25.

At the height of $z=10$ cm, practically no wave-induced power can be found for rpm 200 as seen both from the w'-spectrum in Fig. 30 and from the co- and quad-spectrum in Fig. 23, and the phase lags between u' and w' at that height are nearly 180° at all frequencies, simply showing a feature of the turbulent shear flow. For the case of rpm 300 a small amount of wave-induced power still remains at that height, especially in w' as seen from Fig. 32.

The mean velocity profiles in neutral air over the water waves are also widely believed to be represented by

$$U(z)=\frac{u_*}{\kappa}\log_e\frac{z}{z_0}\,, \tag{14}$$

where $U(z)$: mean wind velocity, z: height above the mean water surface, u_*: friction velocity ($=\sqrt{\tau_0/\rho_a}$), τ_0: wind shear stress at the water surface, ρ_a: density of air, z_0: a constant called 'roughness length', and κ: a constant called 'Karman's constant' usually taken to be 0.4.

The relation (14), which is called log-law, has been well established for the boundary layer over the fixed rough surface; the wind profiles over the fixed surface usually exhibit a good logarithmic portion, which is certainly represented by (14) through the real τ_0, at the height from the surface to 10~20% of the boundary layer (e.g. Clauser, 1956).

On the other hand, this relation has not been confirmed critically for the wind profiles over the water waves and there are still ambiguous problems in applying

this 'log-law' to those wind profiles, especially in a wind-wave tunnel. It is largely becacse there is no means to measure τ_0 at the water surface so accurately as to be able to examine the validity of the relation (14). In the boundary layer over the waves, mean wind profiles can not be measured near the water surface. Even if the wind speed is measured, it is often less accurate because of the large velocity fluctuations than over the solid surface. Moreover it has often been pointed out or discussed that the wind speeds deviate from the log-profile (14) near the water surface (e.g. Stewart (1961), Hamada *et al.* (1963), Mitsuyasu (1964), Phillips (1966), Hamada (1968), etc.). For these reasons there remains the following question to be solved, even if the log-law is applicable to the wind profiles over waves: To what portion of the profiles should the relation (14) be applied to obtain the real u_* (or τ_0)?

Notwithstanding these problems the relation (14) has often been used in order to estimate u_* from the wind profiles (but occasionally in conflicting ways), since u_* is a representative parameter in the experiment of wind and waves and this method is usually the only simple means to obtain it.

One of the main object of the present experiment was to shed some light on the applicability of the log-law to the wind profiles over water waves. This could not be accomplished satisfactorily because of the seasonally inconsistent results in the values of $-\overline{u'w'}$ described before. However we will discuss to the possible extent about the relevant matters mainly on the assumption that the results obtained at the summer season are less reliable than those at the other seasons in the present experiment.

As for the theoretical base of the log-law, it is derived from the mixing-length theory of Prandtl or Karman (e.g. Schlichting (1968)) by presuming the existence of the constant-stress layer next to the boundary but outside the viscous sub-layer, although there are also other derivations from the similarity reasoning (Townsend (1956), Hinze (1959), etc.).

The values of $-\overline{u'w'}$ obtained at the seasons other than summer for each run of both rpm 200 and rpm 300 increased with decreasing height until a certain height z_m where they took the maximum values, and $z_m \fallingdotseq 5 \sim 6$ cm for rpm 200 and $z_m \fallingdotseq 8 \sim 10$ cm for rpm 300 (see Figs. 20 and 21). Below those heights $-\overline{u'w'}$ decreased toward the water surface. However the reduction of $-\overline{u'w'}$ near the wave crests were mostly attributed to the wave-induced Reynolds stress $-\rho_a \tilde{u}\tilde{w}$ as mentioned previously. Taking this into consideration, the turbulent Reynolds stress distribution is regarded as nearly constant over the short distances above the wave crests. Then the wind shear stress acting on the water surface τ_0 is expected to have approximately the same values as the turbulent Reynolds stresses $-\rho_a \overline{u_i' w_i'}$ attained there, which are in turn practically equal to the values of $-\rho_a \overline{u'w'}$ at the height z_m mentioned above. In this way, u_*^2 is expected to be equal to $-\overline{u'w'}$ at the height z_m.

The measurements of the mean wind profiles for rpm 200 were made several times throughout a year similarly to the measurements of velocity fluctuations. Two of those profiles which were measured in winter are shown in Fig. 33-a, b. The profile in Fig. 33-a has a good linear portion, which is indicated by a line there. Applying the relation (14) to this portion, we obtain $u_*=26.6$ cm/sec and consequently $u_*^2=708\,\mathrm{cm^2/sec^2}$. On the other hand, the profile in Fig. 33-b has too much scatter for one to find a suitable straight line for the log-law. It was not rare in our experiments that the scatter of the points in the obtained wind

profiles was as much as that in Fig. 33-b. If we dare to draw a line such as seen in the figure (dotted one), it gives $u_*=22.6$cm/sec and $u_*^2=551\,\text{cm}^2/\text{sec}^2$. Of course this value may include a considerable error, and the results will not be improved very much even if the least square error method is used. We presented the latter profile to illustrate the wrost limit, but not rare in general, of the accuracy of u_* obtained from the wind profiles at the wind speed for rpm 200. Be that as it may, the values of u_*^2 obtained from the two wind profiles are found to be in reasonably good agreement with the values of $-\overline{u'w'}$ obtained at about $z=5$cm (see Fig. 20). Finally we make an additional remark that other two profiles with a good log-linear portion which were measured in summer gave a little larger values of u_*. However its relevance to the seasonal difference of $-\overline{u'w'}$ is not clear.

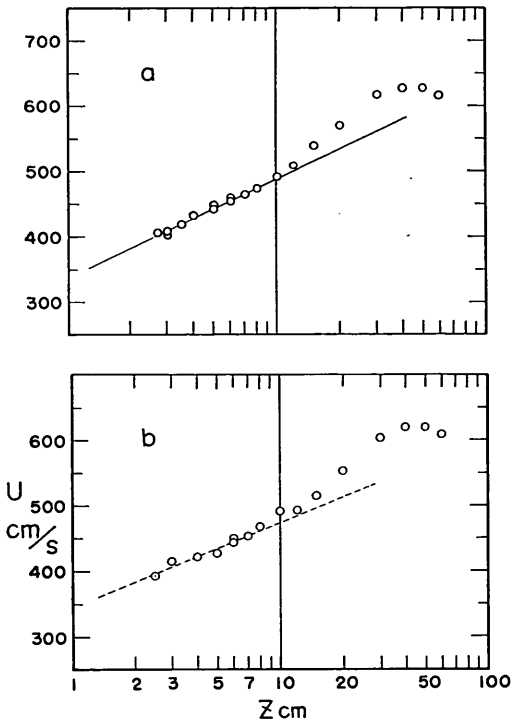

Fig. 33. Wind Velocity Profiles in the cases of wind waves only; rpm 200

On the other hand, the wind profiles for rpm 300 did not show a linear portion so clearly as for rpm 200. A typical wind profile for rpm 300 is shown in Fig. 34. If we attempt to apply the log-law to this kind of profile in order to obtain u_*, it is a problem which portion of the profile to take. One may take the lowest portion, drawing a line such as I in the figure, and another a little higher portion such as II (someone may even take the more higher portion). In the case of Fig. 34, the line I gave $u_*=35.1$ cm/sec, $u_*^2=1230\,\text{cm}^2/\text{sec}^2$, while the line II gave $u_*=43.6$cm/sec, $u_*^2=1900\,\text{cm}^2/\text{sec}^2$. So long as we follow the assumption made earlier, the line I seems to give the better agreement of u_*^2 obtained from the profile with the results of $-\overline{u'w'}$ shown in Fig. 21.

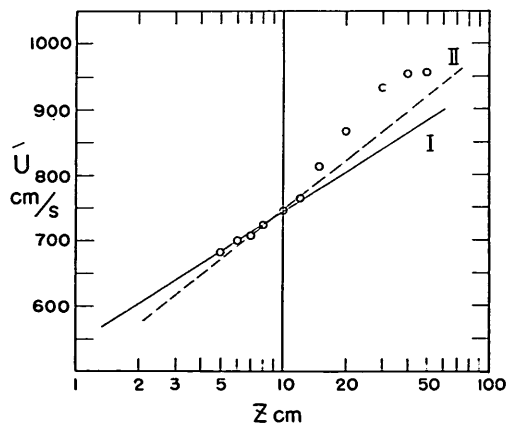

Fig. 34. Wind Velocity Profile in the case of wind waves only; rpm 300

3.3 The Case of Composite Long Waves

The experiment of this case was conducted mainly at the wind speed for rpm 200 ($U_\infty=6.35$ m/sec) and less extensively than the other two cases. The waves were composed of predominant long waves of $T_p=1.60$ seconds and $H\fallingdotseq5.7$ cm which were gen-

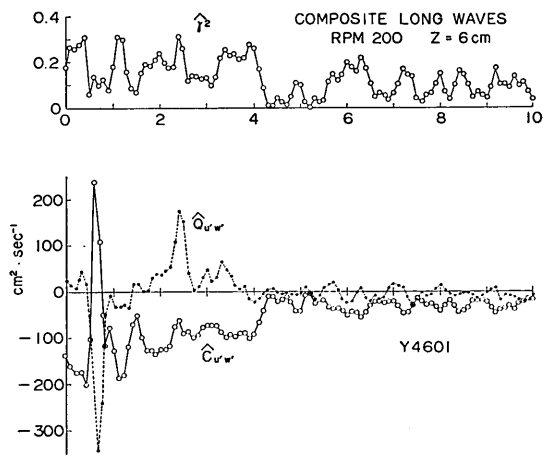

Fig. 35. $u'w'$ Cross-Spectrum in the case of composite long waves; rpm 200, z=6 cm

erated mechanically and smaller wind waves.

Co- and quad-spectra at z=6, 10 and 20 cm, which were obtained in summer, are shown together with the coherences in Figs. 35~37. The results obtained in winter were not different from the results shown in those figures except that the cospectral densities in winter were slightly smaller than those in summer in accordance with the difference in $-\overline{u'w'}$, which will be shown later.

In this case the velocity fluctuations corresponding to the main frequency of wind waves ($f \fallingdotseq 2.5$ Hz) were not found very much either in u'- and w'-spectra or in co- and quad-spectra even at the lowermost measurement height (z=6 cm). On the other hand, the fluctuations induced by the long waves appeared strongly just as in the cases of clear long waves with H=6.0 or 7.0 cm. That is, the co-spectra obtained both in summer and in winter at all measurement heights had a strong positive peak near $f = f_L \fallingdotseq 0.6$ Hz, indicating that there existed a considerable amount of negative wave-induced Reynolds stress. In this case, however, no positive wave-induced stress was found, and this is probably because the

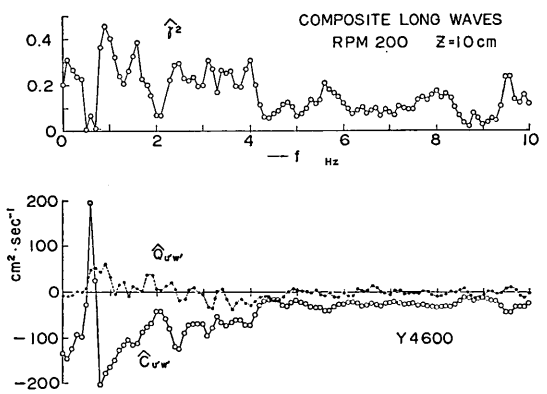

Fig. 36. $u'w'$ Cross-Spectrum in the case of composite long waves; rpm 200, z=10 cm

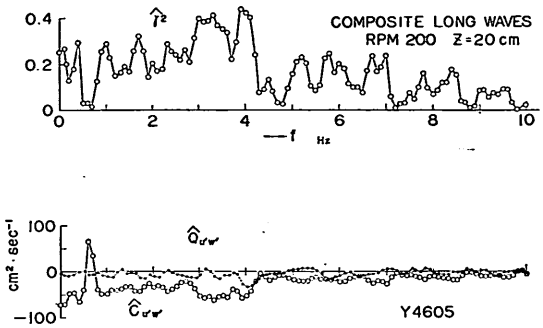

Fig. 37. $u'w'$ Cross-Spectrum in the case of composite long waves; rpm 200, $z=20$ cm

measurement could not be made so close to the mean wave crest as in the cases of clear long waves. One more notable matter is that the coherences $\hat{\gamma}^2$ near $f=0.6$ Hz were extremely small even at $z=6$ cm and the obtained phase lag $\hat{\theta}$ between u' and w' was consequently very unstable (according to Jenkins (1963), the variance of the estimates of phase lag is in proportion to $[(1/\gamma^2)-1]$). This is somewhat in contrast to the cases of clear long waves. At the height $z=40$ cm, however, all turbulent components were remarkably reduced and alternatively the wave-induced components became prominent, producing a high $u'w'$-coherence of $\hat{\gamma}^2=0.9$ at $f\fallingdotseq 0.6$ Hz.

The measurements of u' and w' have also been made by Shemdin & Lai (1970) over the composite long waves ($H=8.64$ cm, $f_L=0.70$ Hz and $c=226$ cm/sec) in a wind-wave tunnel a little larger than that used in our experiments by using hot-film anemometers, and the $u'w'$-cospectra were obtained by means of the analog method. Strange to say, however, there seems to be a definite difference between the results of Shemdin & Lai and ours with respect to the wave-induced Reynolds stresses. In their experiments the cospectrum for $z=10.2$ cm obtained at the fetch 9.15 m for the reference wind speed 10.7 m/sec exhibited a very dominant negative peak at the frequency of the mechanically generated waves $f_L=0.70$ Hz, indicating a large positive wave-induced Reynolds stress. That positive stress distinctly appeared also at the heights of $z=20.3$ cm and $z=50.8$ cm although their absolute values decreased with increasing height. The positive wave-induced stresses were also found at the fetch 25.4 m for the same wind speed.

For the purpose of reference, we made measurements of $u'w'$-cospectra for the higher wind speeds, such as $U_\infty=8.0$, 9.6, 11.3, 12.9 m/sec at the height $z=10$ cm, but only the negative wave-induced Reynolds stresses similar to those in Figs. 35 and 36 were found.

Our results were obtained at the fetch 18.8 m, while those of Shemdin & Lai at the fetch 9.15 m and 25.4 m. It is least probable, however, that the wave-induced Reynolds stresses vary changing their sign alternately with fetch. Then the reason can not be made out why our results differed so seriously from those of Shemdin & Lai (1970).

The values of $-\overline{u'w'}$ obtained from the two different runs conducted in summer and winter, respectively, are shown in Fig. 38 (with dark marks) together with the corresponding results for the cases of wind waves only obtained at the same day (with open marks). The difference of the results between the two

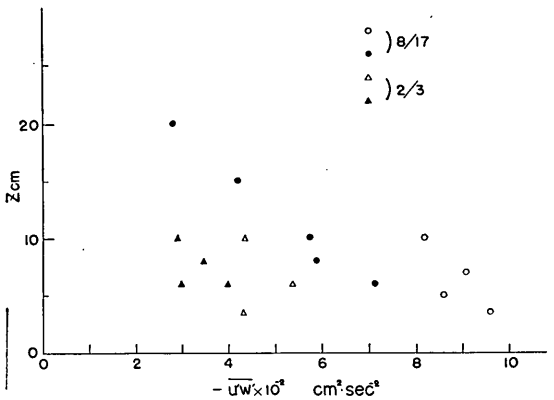

Fig. 38. Distribution of $-\overline{u'w'}$ (rpm 200): ●, ▲—composite long waves; ○, △—wind waves only

seasons is obvious and just the same as in the cases of wind waves only. It is further seen that the values of $-\overline{u'w'}$ for the cases of composite long waves are considerably smaller than those for wind waves only. Of course the negative wave-induced Reynolds stresses existed in the former cases, but their magnitude roughly estimated from the variations of cospectra by the graphical method of Fig. 10 are 60~70 cm²/sec² at most and obviously smaller than the above-mentioned difference between the former and the latter cases. Therefore, the turbulent Reynolds stresses in the former cases seem to be smaller than those in the latter cases at the small heights above the water surface.

4. Conclusions

The measurements have been made of the horizontal and vertical wind velocity fluctuations, u' and w', over the three kind of waves in a wind-wave tunnel by the use of an X-array hot-wire system and the digital method. The main findings obtained are as follows:

1) The existence of the wave-induced velocity fluctuations was found not only in u'- and w'-spectra but also in the cross spectra between u' and w'.

2) It was found that $-\tilde{u}\tilde{w}$ obtained from the variation of cospectra by the graphical method of Fig. 10 gives a reasonably good estimate of the wave-induced Reynolds stresses.

3) In the cases of 'clear long waves', the wave-induced Reynolds stresses definitely existed above the critical layer. When the wave height was small (H=1.1 cm), only the positive wave-induced stresses were found at the small height above the wave crests. For the larger wave heights (H=6.0 or 7.0 cm), however, the negative wave-induced stresses were prevailing over most of the height except slightly above the wave crests where they were positive.

4) In the cases of wind waves only, the wave-induced velocity fluctuations also existed considerably at the lowest height above the wave crests. However they were almost 90° out of phase and did not make much contribution to the $u'w'$-cospectra if any, mostly contributing to the quad-spectra. Nevertheless the cospectra obtained in winter showed signs of the negative wave-induced stresses.

5) In these cases the seasonal differences, not only quantitative but also

qualitative, were found in the values of $-\overline{u'w'}$ especially near the water surface. The results obtained at the seasons other than summer indicated that the turbulent Reynolds stresses are likely to be nearly constant at the small heights above the wave crests. It was further found that those nearly constant stresses are in reasonable agreement with the surface shear stresses estimated by applying the log-law to the lowest portion of the wind velocity profiles.

6) In the cases of composite long waves, only the negative wave-induced Reynolds stresses of non-negligible magnitude were found at all the measurement heights regardless of the season, and the turbulent velocity fluctuations were predominant even at the lowest height somewhat in contrast to the cases of 'clear long waves'.

The authors wish to express their appreciation to Dr. T. Hamada, Chief of Hydraulic Laboratory, for the suggestion of the measurement for the case of smaller wave height and for the critisisms given in the course of preparation of this report. The digital computations have been conducted by the use of a digital computor TOSBAC 3400 at the Computation Center of the Port and Harbour Research Institute, and the thanks are also due to Messrs. N. Ogawa and M. Tsubata, members of the Computation Center, for the arrangements offered to the authors mainly in the connection of the digital data recorder with the computer.

References

1) BARNETT, T. P. and WILKERSON, J. C. (1967): On the generation of wind waves as inferred from airbone radar measurement of fetch limited spectra, *J. Mar. Res.*, 25, 292-328.
2) BLACKMAN, R. B. and TUKEY, J. W. (1958): *The measurement of power spectra*, Dover Publications, New York.
3) CLAUSER, F. H. (1956): The turbulent boundary layer, *Adv. in Appl. Mech.*, 4, 1-51, Academic Press.
4) HAMADA, T., SHIBAYAMA, A. and KATO, H. (1963): An experimental study of development of wind waves, *Rep. of Port and Harbour Res. Inst.*, No. 2, p. 41.
5) HAMADA, T. (1968): On some properties of wind over water waves (in Japanese), *Rep. of Port and Harbour Res. Inst.*, Vol. 7, No. 4, 3-22.
6) HINZE, J. O. (1959): *Turbulence*, McGraw-Hill Book Co.
7) JEFFREYS, H. (1924): On the formation of water waves by wind, *Proc. Roy. Soc.* A, **107**, 189-206.
8) JEFFREYS, H. (1925): On the formation of water waves by wind, II, *Proc. Roy. Soc.* A, **110**, 241-247.
9) JENKINS, G. M. (1963): Cross-Spectral Analysis and the Estimation of Linear Open Loop Transfer Functions, *Time Series Analysis*, John Wiley & Sons, Inc., 267-276.
10) KATO, H. and TAKEMURA, K. (1966): Wind profiles over the shallow water (1st Report) (in Japanese), *Rep. of Port and Harbour Res. Inst.*, Vol. 5, No. 1, 1-21.
11) KATO, H. and SANO, K. (1969): Measurements of Wind Velocity Fluctuations over Waves in a Wind-Wave Tunnel, *Rep. of Port and Harbour Res. Inst.*, Vol. 8, No. 1, 3-35.
12) KENDALL, J. M. (1970): The turbulent boundary layes over a wall with progressive surface waves, *J. Fluid Mech.*, 41, 259-281.
13) MILES, J. W. (1957): On the generation of surface waves by shear flows, *J. Fluid Mech.*, 3, 185-204.
14) MILES, J. W. (1967): On the generation of surface waves by shear flows, Part 5, *J. Fluid Mech.*, 30, 163-175.

15) MITSUYASU, H. (1964): Wind shear stress at the water surface and the surface roughness (in Japanese), *Proc. 11th Japanese Conf. Coast. Eng.*, 42-48.
16) MOTZFELD, H. (1937): Die turbulente Strömung an welligen Wänden, *Z. angew. Math. Mech.*, **17**, 193-212.
17) PHILLIPS, O. M. (1957): On the generation of waves by turbulent wind, *J. Fluid Mech.*, **2**, 417-445.
18) PHILLIPS, O. M. (1966): *The Dynamics of the Upper Ocean*, Cambridge Univ. Press., p. 261.
19) POND, S., STEWART, R. W. and BURLING, R. W. (1963): Turbulence spectra in the wind over waves, *J. Atmos. Sci.*, **20**, 319-324.
20) POND, S., SMITH, S. D., HAMBLIN, D. F. and BURLING, R. W. (1966): Spectra of velocity and temperature fluctuations in the atmospheric boundary layer over the sea, *J. Atmos. Sci.*, **23**, 376-386.
21) SCHLICHTING, H. (1968): *Boundary-Layer Theory*, 6th Ed., McGraw-Hill Book Co.
22) SHEMDIN, O. H. and LAI, R. J. (1970): Laboratory Investigation of Wave-Induced Motion above Air-Sea Interface, *Dept. of Coastal and Oceanographic Engineering, Tech. Rep., No. 6, Univ. of Florida*, Gainesville.
23) SMITH, S. D. (1967): Thrust anemometer measurements of wind-velocity spectra and of Reynolds stress over a coastal inlet, *J. Mar. Res.*, **25**, 239-262.
24) SNYDER, R. L. and COX, C. S. (1966): A field study of the wind generation of ocean waves, *J. Mar. Res.*, **24**, 141-178.
25) STANTON, T. E., MARSHALL, D. and HOUGHTON, R. (1932): The growth of waves on water due to the action of the wind, *Proc. Roy. Soc.* A, **137**, 283-293.
26) STEWART, R. W. (1961): The wave drag of wind over water, *J. Fluid Mech.*, **10**, 189-194.
27) STEWART, R. W. (1967): Mechanics of the air-sea interface, *Phys. Fluids* **10**, *Supplement on boundary layers and turbulence*, S47-S55.
28) WEILER, H. S. and BURLING, R. W. (1967): Direct measurements of stress and spectra of turbulence in the boundary layer over the sea, *J. Atmos. Sci.*, **24**, 653-664.

(Received 27 December 1970)

List of Symbols

a_1: hot-wire constant (cf. Eq. 1)
c: phase velocity of periodic waves
E: output voltage from a hot-wire anemometer
E_0: hot-wire constant (cf. Eq. 1)
$\hat{C}_{u'w'}(f)$: cospectral density between u' and w'
f: frequency
f_L: frequency of the mechanically generated waves
f_N: holding frequency in the spectral computations
f_p: frequency at which a wave spectrum shows the maximum density
Δf: frequency resolution in the spectral computations
h: maximum lag in the spectral computations
H: crest-to-trough wave height
$H_{1/3}$: significant wave height estimated from the total power of the wave spectra
K: conversion coefficient (cf. Eq. 2)
M: total output voltage from a linearlizer
N: total number of the data used in a computation
$\hat{Q}_{u'w'}(f)$: quad-spectral density between u' and w'
$r_a(f)$: attenuation factor for the 3-point array
$r_s(f)$: attenuation factor for the 3-point sliding mean
rpm: revolution number of the blower's fan per minute
t_i: time position corresponding to a particular wave phase
Δt: data sampling time interval
T_p: wave period
ΔT: temperature difference between air (in the laboratory) and water
ΔT_1: temperature difference of flowing air between near the water surface and at $z=40$ cm
u': total horizontal (streamwise) velocity fluctuations ($=\tilde{u}+u_t'$)
$\tilde{u}$: horizontal wave-induced velocity fluctuations ($=\langle u' \rangle$)
u_t': horizontal turbulent velocity fluctuations
u_*: friction velocity ($=\sqrt{\tau_0/\rho_a}$)
U: mean wind speed
U_∞: maximum wind speed
w': total vertical velocity fluctuations ($=\tilde{w}+w_t'$)
$\tilde{w}$: vertical wave-induced velocity fluctuations ($=\langle w' \rangle$)
w_t': vertical turbulent velocity fluctuations
V: normal wind speed to a hot-wire
$-\overline{\tilde{u}\tilde{w}}$: wave-induced Reynolds stress divided by ρ_a
$-\overline{u_t'w_t'}$: turbulent Reynolds stress divided by ρ_a
X, Y: total output voltages from an X-array hot-wire system, X corresponding to a wire A in Fig. 2
X', Y': fluctuating part of X and Y, respectively
z: height above the mean water surface
z_m: height at which $-\overline{u'w'}$ takes the maximum value
z_0: roughness length
—: upper bar denoting overall time average

$\langle\ \rangle_\varepsilon$: time average with respect to a particular wave phase
$\langle\ \rangle$: equivalent to $\langle\ \rangle_\varepsilon$
α', β': constants determined from the hot-wire calibration curves
α, β: constants ($\alpha=\alpha'/\sqrt{2}$, $\beta=\beta'/\sqrt{2}$)
$\hat{\gamma}^2$: coherence between u' and w'
ε: subscript referring to a particular wave phase
κ: Karman's constant ($\fallingdotseq 0.4$)
$\hat{\theta}$: phase lag of the w'-data relative to the u'data
ρ_a: density of air
τ_0: wind shear stress at the water surface
$\Delta\tau$: original sampling time interval for the 3-point sliding mean

Appendix

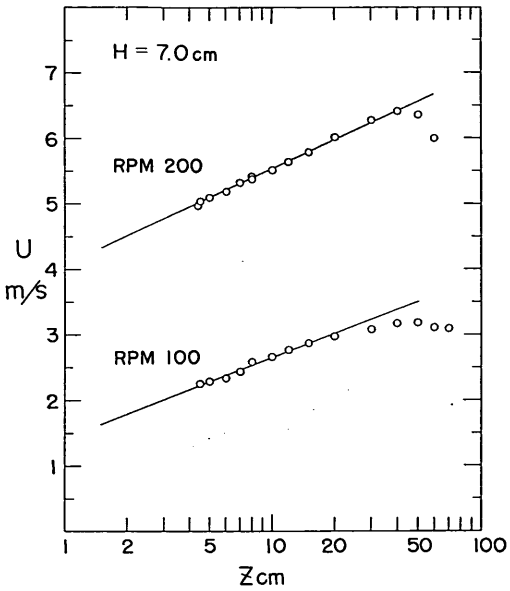

Fig. A-1. Wind Velocity Profiles in the cases of clear long waves; rpm 200 & 100, H=7.0 cm

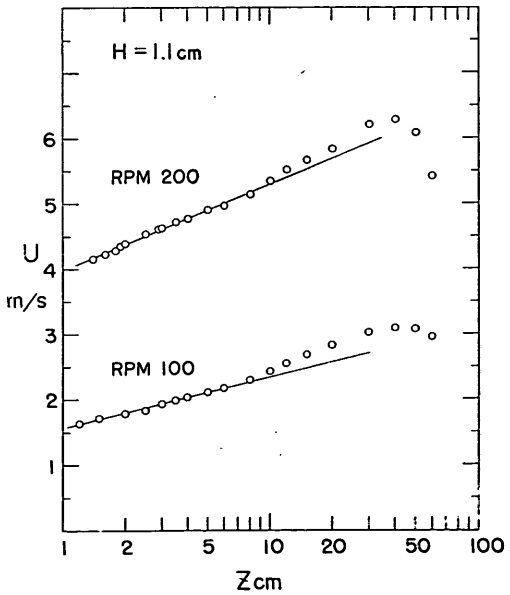

Fig. A-2. Wind Velocity Profiles in the cases of clear long waves; rpm 200 & 100, H=1.14 cm

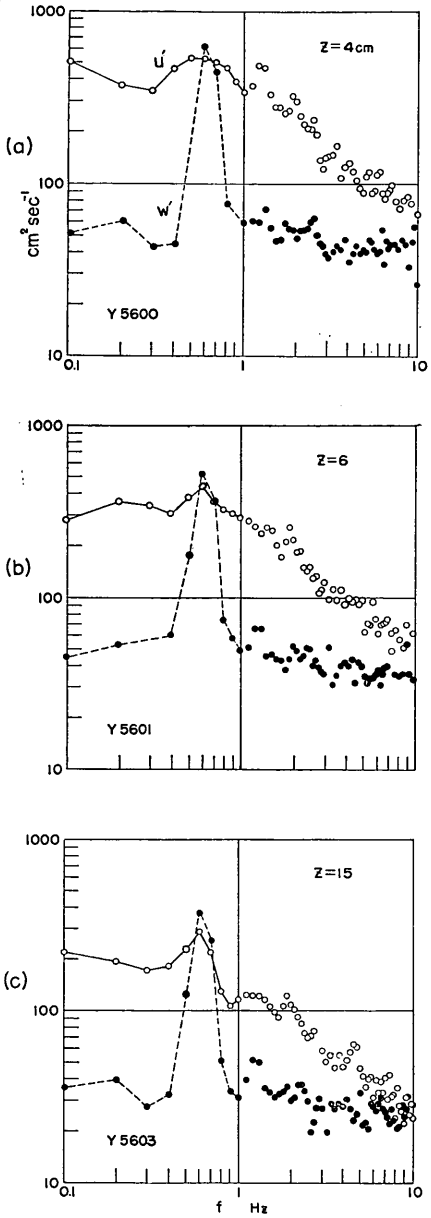

Fig. A-3. u'- and w'-Spectra in the cases of clear long waves; rpm 200, H=6.0 cm

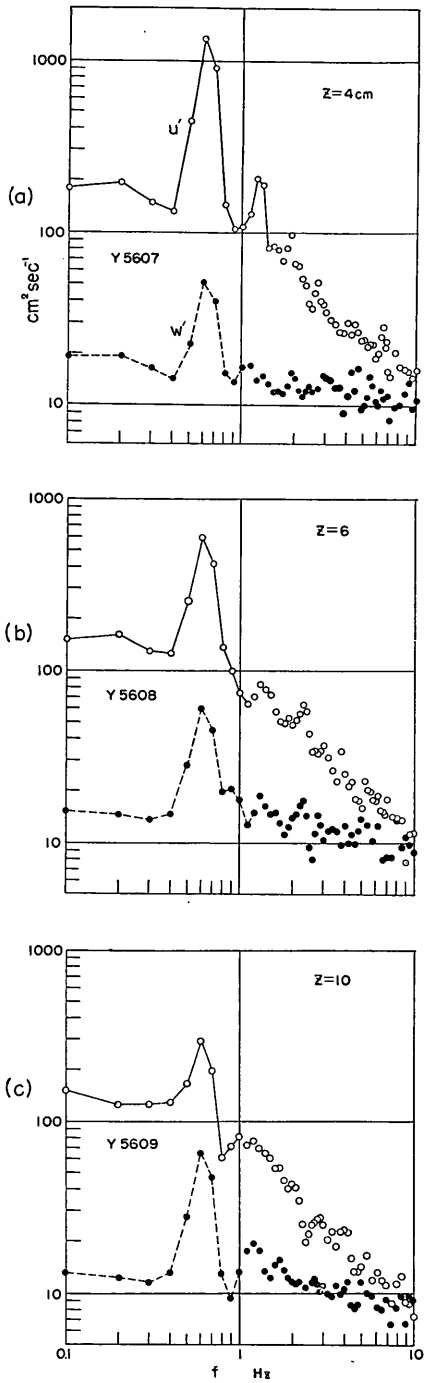

Fig. A-4. u'- and w'-Spectra in the cases of clear long waves; rpm 100, H=6.0 cm

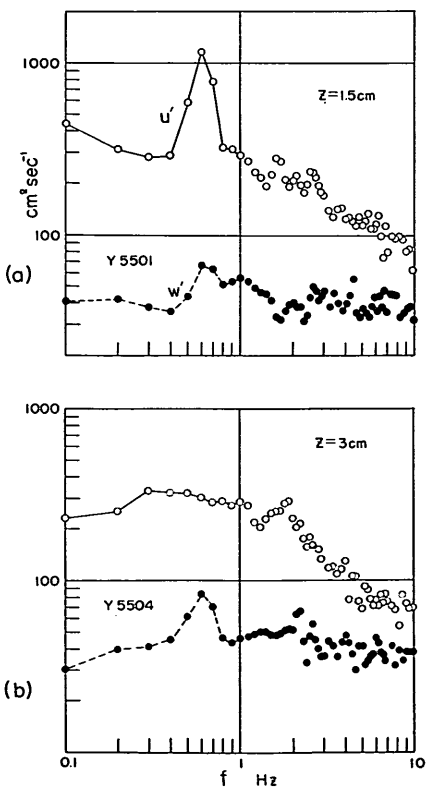

Fig. A-5. u'- and w'-Spectra in the cases of clear long waves; rpm 200, H=1.14 cm

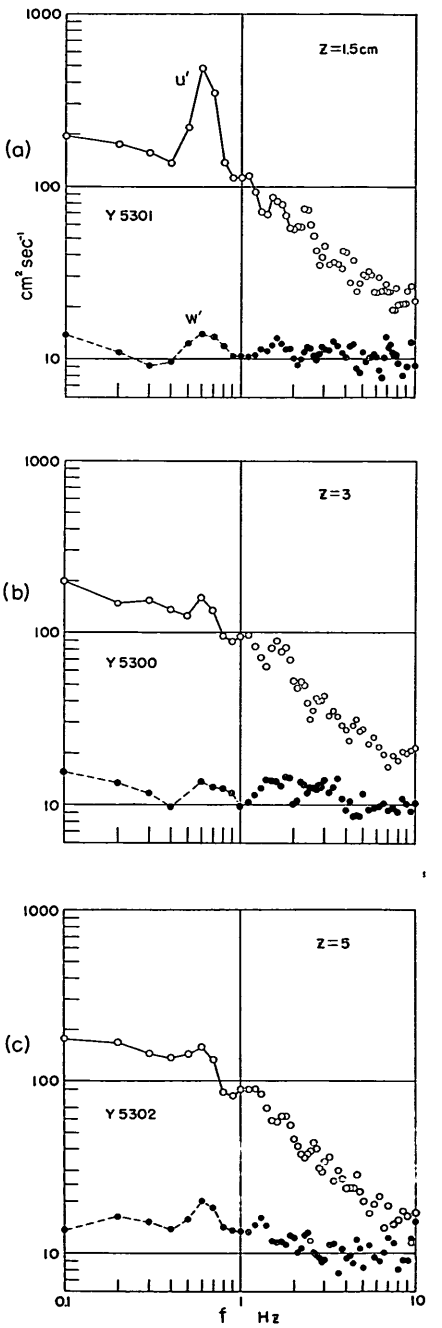

Fig. A-6. u'- and w'-Spectra in the cases of clear long waves; rpm 100, H=1.14 cm

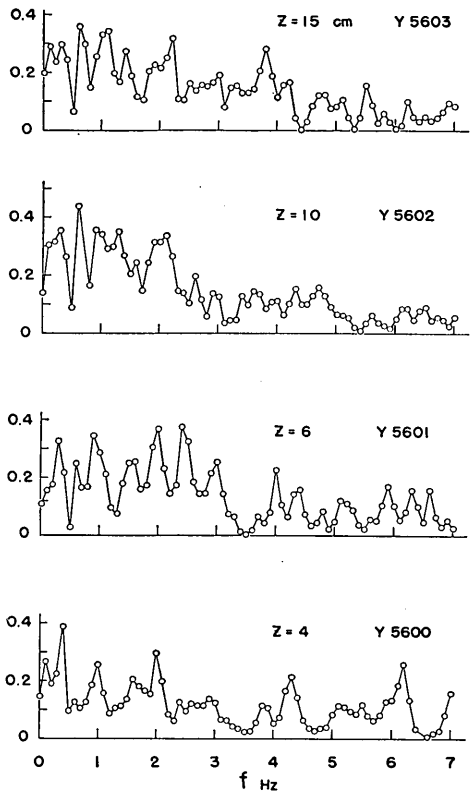

Fig. A-7. $u'w'$ Coherences for the cases of Fig. 5 (rpm 200 & H=6.0 cm)

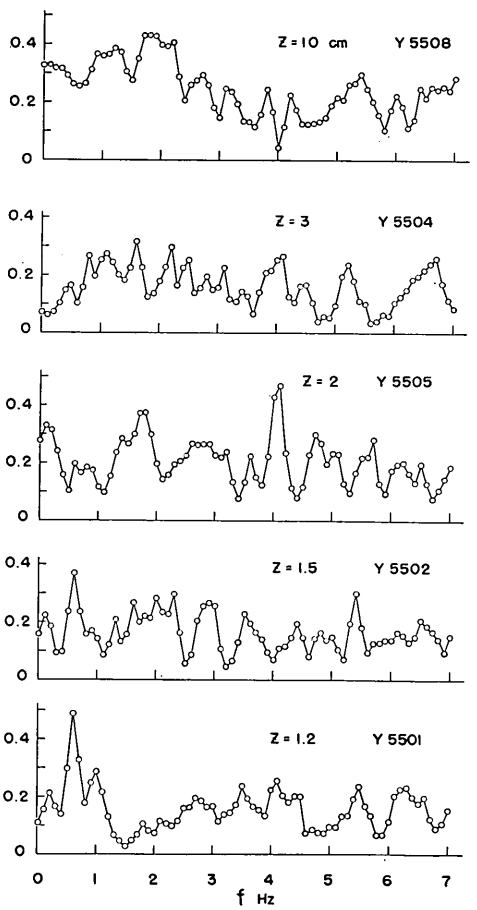

Fig. A-8. $u'w'$ Coherences for the cases of Fig. 6 (rpm 200 & H=1.14 cm)

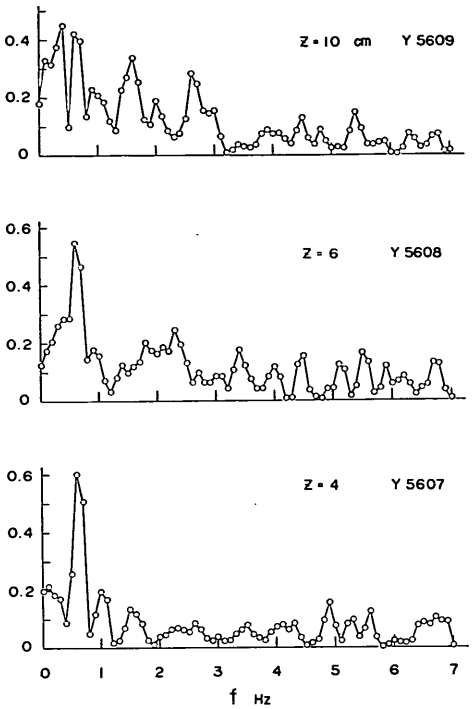

Fig. A-9. $u'w'$ Coherences for the cases of Fig. 7 (rpm 100 & H=6.0 cm)

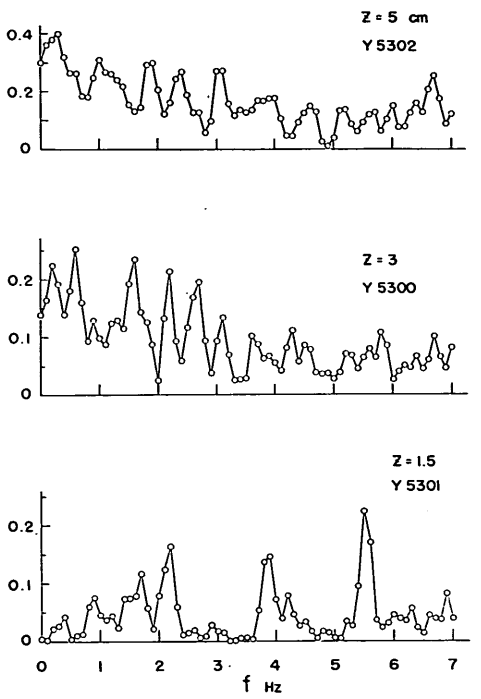

Fig. A-10. $u'w'$ Coherences for the cases of Fig. 8 (rpm 100 & H=1.14 cm)

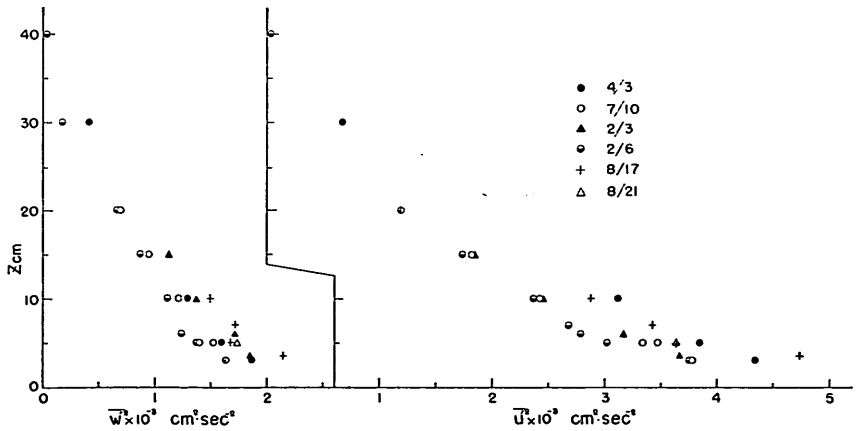

Fig. A-11. Distributions of $\overline{w'^2}$ and $\overline{u'^2}$ in the cases of wind waves only, rpm 200

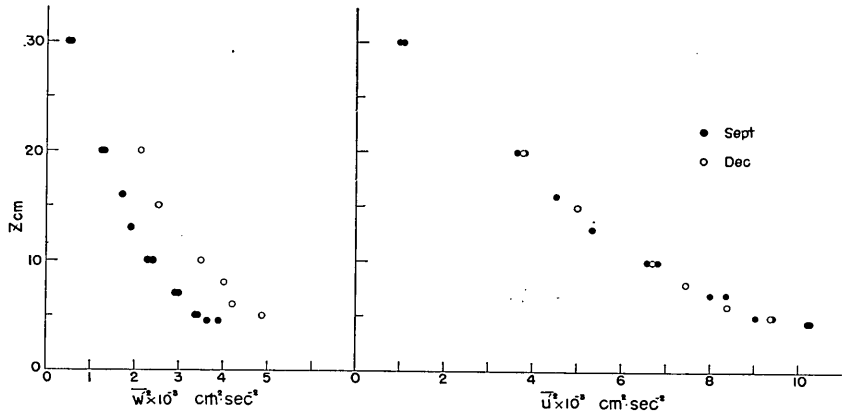

Fig. A-12. Distributions of $\overline{w'^2}$ and $\overline{u'^2}$ in the cases of wind waves only, rpm 300

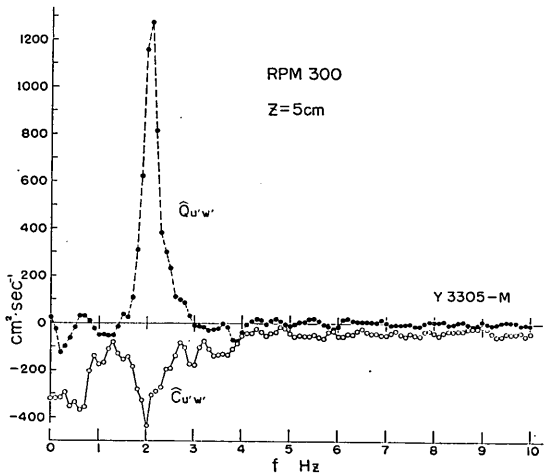

Fig. A-13. Co- and Quad-Spectrum in the case of wind waves only, at z=5 cm, rpm 300